Greta Bajni · Corrado A. S. Camera · Tiziana Apuani

Deciphering meteorological influencing factors for Alpine rockfalls: a case study in Aosta Valley

Abstract This study exploited the historical rockfall inventory and the meteorological stations database of Mont Cervin and Mont Emilius Mountain Communities (Aosta Valley, northern Italy) to decipher relationships between climate processes, typical of mountain environments and rockfall phenomena. The period from 1990 to 2018 was selected as reference to perform the analysis. Climate processes were translated into four climate indices, namely short-term rainfall (STR), effective water inputs (EWI, including both rainfall and snow melting), wet and dry episodes (WD) and freeze-thaw cycles (FT). The comparison between climate indices values at each rockfall occurrence and the statistical distributions describing the whole indices dataset allowed to define not ordinary climatic conditions for each index and their influence on rockfall occurrence. Most of the events analysed (>95% out of 136) occurred in correspondence of the defined not ordinary climatic conditions for one or for a combination of the indices. The relationships between rockfalls and climate showed a seasonality. In spring, most of the events resulted to be connected to FT (70%) while in autumn to EWI (49%). The relative seasonal importance of WD reached its maximum in summer with 23% of the events related to this index alone. Based on these results, different strategies to define empirical critical thresholds for each climate index were explored, in order to make them valid for the whole study area. A preliminary exploratory analysis of the influence of high temperatures and temperature gradients was carried out for some summertime rockfalls, not correlated to the other investigated indices. The presented approach is exportable in neighbouring regions, given the availability of a dated rockfall dataset, and could be adapted to include different processes.

Keywords Rockfall · Climate indices · Cumulated precipitation · Wet-dry episodes · Freeze-thaw cycles · Threshold

Introduction

Rockfalls are a common type of fast-moving landslide (Hungr et al. 2014). As such, they can deeply affect human society and infrastructures in mountainous environments (Ravanel and Deline 2010, Duvillard et al. 2015, Scavia et al. 2020). Also, they are a very challenging type of landslides to predict, since their occurrence is related to both geomechanical (e.g. rock type, in situ stress, fracture network characteristics) and meteorological characteristics (e.g. intense rainfall events, prolonged precipitation periods, freeze-thaw cycles), which are extremely variable over space and time (Scavia et al. 2020). In the Alpine region, their effects are expected to exacerbate under climate change (Crozier 2010; Stoffel et al. 2014). In recent years, the main approaches adopted to decipher rock mass instability dynamics are crack kinematics analysis and quantification of timing-frequency-volume of rockfall events. Matsuoka (2001, 2008), Hasler et al. (2012) and Weber et al. (2017) analysed crack kinematics with extensometers and crackmeters. For the same purpose, Amitrano et al. (2010, 2012), Krautblatter and Draebing (2014), Zimmer and Sitar (2015) and

Draebing et al. (2017b) applied seismic, acoustic and geoelectrical techniques. For the quantification of timing-frequency-volume of rockfall events, Matsuoka (2013) employed time-lapse cameras, Krautblatter and Moser (2009) used traps, while Ravanel et al. (2013) and Hartmeyer et al. (2020) used terrestrial laser scanners. These acquisition methods, and the exploitation of accurate historical and multitemporal (i.e. inventories prepared for the same area but for different time periods, as defined by Reichenbach et al. (2018)) rockfall inventories, are often combined with the monitoring and analysis of meteorological data to evaluate preparatory and triggering factors for rockfall occurrence (Delonca et al. 2014; D'Amato et al. 2016; Paranunzio et al. 2015, 2016, 2019; Draebing et al. 2017a; Nigrelli et al. 2018; Matsuoka 2019).

Rainfall processes related to rock slope instability include (i) rising of water pressure in joints with a consequent reduction of shear strength; (ii) joint clayey infilling swelling, dissolution and leaching with a consequent reduction in joint cohesion; and (iii) reduction of the strength of rock bridges for some rock masses. These processes could act at different timescales, depending on the intensity and duration of the rainfall events.

Temperature variations can affect rock mass properties as well. Given partially saturated joints, temperature can deteriorate rock masses through transitions across 0 °C (i.e. freeze-thaw cycles). Freeze-thaw cycles affect rock masses through both ice formation-melting processes (i.e. frost cracking and frost weathering, Hales and Roering 2007; Matsuoka 2008), which, acting on the long-term, enable ice segregation-induced subcritical cracking, progressively decreasing rockwalls strength (Draebing and Krautblatter 2019) and rock thermal weathering (i.e. repeated expansion and contraction leading to rock mass fatigue). Even a negative warming can induce crack propagation due to the thermal expansion of ice (i.e. thermal wedging, D'Amato et al. 2016). Furthermore, positive temperatures and gradients both lead to ice melting and thus to a loss of cohesion. In the light of global warming, an interest in analysing the role of positive temperatures on rockfall occurrence is spreading in the scientific community. In arid and semiarid environments, very high positive temperatures (up to 40°C) could lead to rock mass exfoliation and fracturing through thermal stress cycles (Bakun-Mazor et al. 2013; Vargas et al. 2013; Collins and Stock 2016; Collins et al. 2018). Conversely, the authors working on Alpine rockfalls recognized the role of extremely warm temperatures principally on permafrost degradation and snow melt dynamics, which lead to an increasing water availability and circulation in rock joints (Allen and Huggel 2013; Bodin et al. 2015; Paranunzio et al. 2016; Nigrelli et al. 2018). Nonetheless, in Alpine environments, thermal stress weathering is principally related to the occurrence of the transition above/below 0 °C (Nigrelli et al. 2018).

The wet-dry cycles are another important rockfall climate-related preparatory factor that is often neglected at the slope scale but frequently investigated at the lab scale (Van der Hoven et al. 2003; Torres-Suarez et al. 2014; Zhou et al. 2017; Yang et al. 2018,

2019). Water can interact with rocks through pores, fissures and microdefects, resulting in changes in several microstructural characteristics. The rock microstructure damages have a macroscopic manifestation in the deterioration of mechanical properties and the increase in deformation of rock masses. The damage caused to rock masses by multiple cycles is gradually accumulated and irreversible. The weakening effect of these cycles on rocks is often stronger than that of being soaked in water for a long time, and thus it seriously influences the long-term stability of rock masses (Yang et al. 2018).

Previous studies focusing on the interaction between rockfalls and meteorological events (e.g. Matsuoka 2019; Paranunzio et al. 2019) highlighted the extreme variability of these relationships; the authors mostly investigated short-term effects related to rainfall (i.e. rainfall intensity and amount at the sub-daily, daily or weekly scale) or long-term effects related to freeze-thaw cycles and temperature extremes (i.e. at the monthly, quarterly or longer period scale). Their findings testify that both the short-term and long-term effects should not be neglected, representing triggering and preparatory factors for rockfall instability, respectively. Triggering factors are immediate causes acting directly, while preparatory factors are linked to a slow cumulative effect, requiring a higher amount of time to induce a major consequence (Gunzburger et al. 2005).

In the Japanese Alps, Matsuoka (2019) identified five key climate-related processes controlling rockfall occurrence: (i) summer and early autumn heavy rainfall events; (ii) lighter, repeated rainfall events leading to a moisture increase followed by freeze-thaw cycles, occurring primarily in spring and autumn; (iii) same as (ii) but with snowfall replacing rainfall, in winter and early spring; (iv) seasonal thawing after deep winter freezing; and (v) thermal stress induced by large thermal fluctuations (mainly in winter). In the Italian Alps, Paranunzio et al. (2015, 2016, 2019) proposed an approach to decipher climate anomalies associated with the occurrence of rockfalls at high elevations. The approach includes the analysis of temperature, temperature variations and rainfall data by comparing the values observed for these climatic variables before rockfall occurrences with the empirical distribution function of a reference sample. To derive the latter, all the available values recorded for the climate variables in the same period of the year with different temporal aggregations are used. They found different positive and negative anomalies (i.e. values corresponding to the tails of the distribution) associated to rockfall occurrence. In particular, at elevations between 1500 and 2400 m a.s.l., rockfalls occurred mainly in spring and were mostly associated with negative temperature anomalies. At high elevations (above 2400 m a.s.l.), rockfall events concentrated in summer and positive temperature anomalies prevailed as triggering conditions. Only 15% of the rockfalls recorded in the database were associated with exceptional precipitation in the 7–90 days preceding failure. During 4 years of rockfall measurements by means of nets and traps in the German Alps, Krautblatter and Moser (2009) found that rockfall intensity is only coupled to rainfall intensity above a certain threshold (i.e. 9–13 mm/30 min) and that the rockfall response to rainfall intensity above the threshold is highly nonlinear. In the French Alps, D'amato et al. (2016) quantified that the highest daily-weekly rockfall frequency of a rock wall near Grenoble occurred during freeze-thaw cycles, especially during thawing periods, but the highest hourly rockfall frequency

occurred during intense rainfalls (more than 5 mmh $^{-1}$). In another study area of France, Delonca et al. (2014) observed that the most influential parameter leading to an increase in rockfall frequency is the cumulated rainfall in the antecedent 3-day period. In Switzerland, Strunden et al. (2015) compared different size groups of rockfall events with environmental factors (e.g. freeze-thaw cycles, temperature, precipitation and seismicity) using a linear regression with variable lag times between 0 and 6 months. The highest correlation factor was observed for freeze-thaw cycles and rockfall events involving volumes smaller than 1 m^3 with a 2-month delay between temperature extremes and rockfalls. A rather high correlation was discovered between cumulated precipitation and rockfall events for a 4- to 6-month lag time, too. Along a railway section through the Canadian Cordillera, Macciotta et al. (2015) found that the seasonal variation in rockfall frequency was mostly associated with cycles of freezing and thawing during the winter months. They also compared the intensity of precipitation and freeze-thaw cycles for different time windows against recorded rockfalls and used their findings to propose a rockfall hazard chart. In Aosta Valley, Ponziani et al. (2020) analysed the relationship between debris flows and the dynamics of freezing level, permafrost temperature and rainfall, in order to account for these hydro-meteorological processes in the regional early warning system.

Studies regarding the influence of climate factors allow to design triggering thresholds. A threshold is a curve that may define the conditions that, when reached or exceeded, are likely to trigger landslides. Thresholds can be defined on physical or empirical bases. Intensity-duration thresholds for landslide initiation are the most common type in literature (Guzzetti et al. 2007 and references therein). They usually have the form of a negative power law:

$$I = c + \alpha D^{\beta} \tag{1}$$

where I is the rainfall intensity, D is rainfall duration and c (≥ 0), α, and β are empirical parameters. They are very common for shallow landslides, and only in few cases they consider other types of mass movements, including rockfalls. Reasons are the easily detectable relationships between shallow landslides and extreme meteorological events and their occurrence on gentler and less remote slopes in comparison to those affected by rockfall. Furthermore, quantitative thresholds regarding freeze-thaw or wet-dry cycles are very rare in the related literature; e.g. D'Amato et al. (2016) quantified that rockfall frequency can be multiplied by a factor of 7 during freeze-thaw episodes.

Despite the presented studies and approaches, many authors agree that more research is needed to improve the understanding of the relationships between climate variables variability and geo-hydrological hazards. Additional knowledge on these relationships is fundamental to elaborate adaptation strategies for the prevention and the mitigation of climate change impacts in mountainous environments (Crozier 2010; Stoffel et al. 2014; Gariano and Guzzetti 2016). The general aim of this study is to define a procedure to recognize climate conditions influencing rockfall occurrence in an Alpine environment, combining both their critical short-term (triggering) and long-term (preparatory) effects. The

study focuses over the Mountain Communities of Mont Cervin and Mont Emilius (Aosta Valley, Western Italian Alps), where a large historical rockfall inventory and an extensive, multivariable meteorological dataset are available for the period 1990–2018 (i.e. a three-decade period allowing the calculation of *Climate Normals* as defined by the World Meteorological Organization (1989, 2007)). In detail, the study will investigate the relationships between rockfall occurrences and four climatic indices, addressing several temporal scales: (1) short-term rainfall (sub-daily data), (2) effective water inputs (daily data, both considering rainfall and snow melting), (3) wet-dry episodes and (4) freeze-thaw cycles. For this purpose, specific sub-objectives were developed: (i) validation of the rockfall inventory, (ii) pre-processing of the climatic dataset to ensure different stations data comparability and a uniform usability, (iii) calculation of the statistical distribution of the four rockfall-related climate indices in the reference period and (iv) definition of empirical critical thresholds for each climate index.

Study area

Aosta Valley is located in the North Western Italian Alps. It is the smallest Italian region, with an area of 3262 km² (Fig. 1a). The region represents one of the main Alpine valley systems and comprises some of the highest mountain peaks of the Alps, among which Mont Blanc (4810 m a.s.l.), Monte Rosa (4634 m a.s.l.), Matterhorn (4478 m a.s.l.) and Gran Paradiso (4061 m a.s.l.). Due to its complex orography and extremely variable altitude range, the region is characterized by different climate regimes. According to the Köppen's climate classification (Fig. 1c) (Rubel et al. 2017 and reference therein), the climate of the area is classified as Alpine Frost (EF) and Alpine Tundra (ET) at higher elevations, as Boreal with warm summer (Dfb) in the central sector and on the slopes, as Warm Temperate (Cfb) along the secondary valley bottoms (mainly oriented N-S) and arid-semiarid (Bsk) in the eastern-central part of the Dora Baltea Valley bottom (E-W oriented).

The Aosta Valley geological setting is the outcome of the collision of three main continental domains, namely the European palaeomargin, the Briançonnais microcontinent and the Adriatic palaeomargin, originally separated by the Valaisan and the Piedmont-Ligurian oceans. Following the Alpine orogenesis, this complex overlapping structure was interested by a neo-tectonic brittle dislocation system represented by the Aosta-Ranzola fault system. Since it represents a complete section of the Alpine orogenic prism, this sector of the Alpine chain has been extensively studied and analysed starting from the early 1990s (Argand 1911). A detailed and extensive geo-structural characterization of the area is provided by Dal Piaz et al. (2001), Ellero and Loprieno (2017) and references therein. The complex structural-geological context of the region deeply influenced the relief evolution and the slope dynamics. Superimposed to the tectonic evolution, the glacial morpho-dynamics—the region is the one with the largest glacierized area of Italy—have been influencing the slope setting, mainly due to the debuttressing caused by glaciers retreat (Giordan et al. 2018). Gravitational phenomena—shallow landslides, rockfalls and large instabilities—played a fundamental role in shaping the geomorphology of the region. Rockfalls are highly frequent and represent a serious geo-environmental risk in the study area, crossed by the principal highway connecting Aosta to Piedmont region in the south and to Switzerland, France, and the highly popular and frequented area of Valtournenche (Cervinia Ski Area) in the North.

Within the Aosta Valley region, the study area comprehends the Mountain Communities of Mont Cervin and Mont Emilius, which cover an area of 670 km² (bordered in Fig. 1b). The selection of this area is related to the availability of a suitable dataset of rockfalls and weather station spatial-temporal coverage. The area covers an altitude range between 400 and 4500 m a.s.l., developing from the southern massifs to the northern peaks of the region, and passing through the valley bottom nearby Aosta. Moreover, Mt Emilius main valley axis is E-W oriented, whereas Mt Cervin main valley axis is N-S oriented. Local factors such as orientation, inclination, location, land cover, snow cover and human infrastructures play an important role in the climatic and environmental local variability. The study area of the Mont Cervin and Mont Emilius Mountain Communities is characterized by the presence of different lithologies belonging prevalently to the ophiolitic Piedmont zone and Austroalpine outliers (both lower and upper).

Materials and methods

Rockfall dataset

The major limitation related to landslide inventories lays in the well-known inherent incompleteness of non-instrumental historical records of natural events (Guzzetti 2000). The actual Aosta Valley landslide inventory "Catasto Dissesti Regionale SCT", publicly available at http://catastodissesti.partout.it/, represents the result of the integration of different sources, deriving from the evolution of the acquisition methods adopted. During the 1990s, landslides information was recorded only qualitatively from different regional offices or scientific organizations. The great flood event of the Western Alps, occurred between 13 and 16 October 2000 (Ratto et al. 2003), represented a starting point for the regional authority to implement a more organized and structured landslide inventory, which comprised cartographic and quantitative information. During 2001–2004, Aosta Valley adhered to the construction of the Italian Landslide Inventory, named IFFI (Inventario dei Fenomeni Franosi in Italia, http://www.progettoiffi.isprambiente.it/cartografia-on-line/). From 2005, the regional database was enriched through field work and orthophotos observations. Even the historical phenomena and great paleo-events were further analysed and validated. Since 2010, the regional landslide inventory has been regularly updated thanks to an innovative automatic computerized data acquisition procedure, involving both the Regional Civil Protection Department and the Forest Corps operating in the territory.

Rockfall-related data were extracted and thoroughly checked (Fig. 1d) for errors, duplicated values and the identification of source areas when only deposit coordinates were recorded. In detail, each rockfall record was validated by consulting the Digital Terrain Model, orthophotos, geological and geomorphological maps available for the area (http://geoportale.regione.vda.it/), searching for source areas evidences (e.g. outcrops, scarps and rock walls). Once validated, each record was associated with a unique ID. For the study reference period (1990–2018), histograms of rockfall occurrence per year and per month were produced. The former was used to analyse the number of recorded phenomena as a function of the acquisition method through time, and the latter was expected to highlight possible seasonal patterns. A non-parametric analysis of the rockfall volumes was also carried out by means of histogram-based frequency and of the empirical
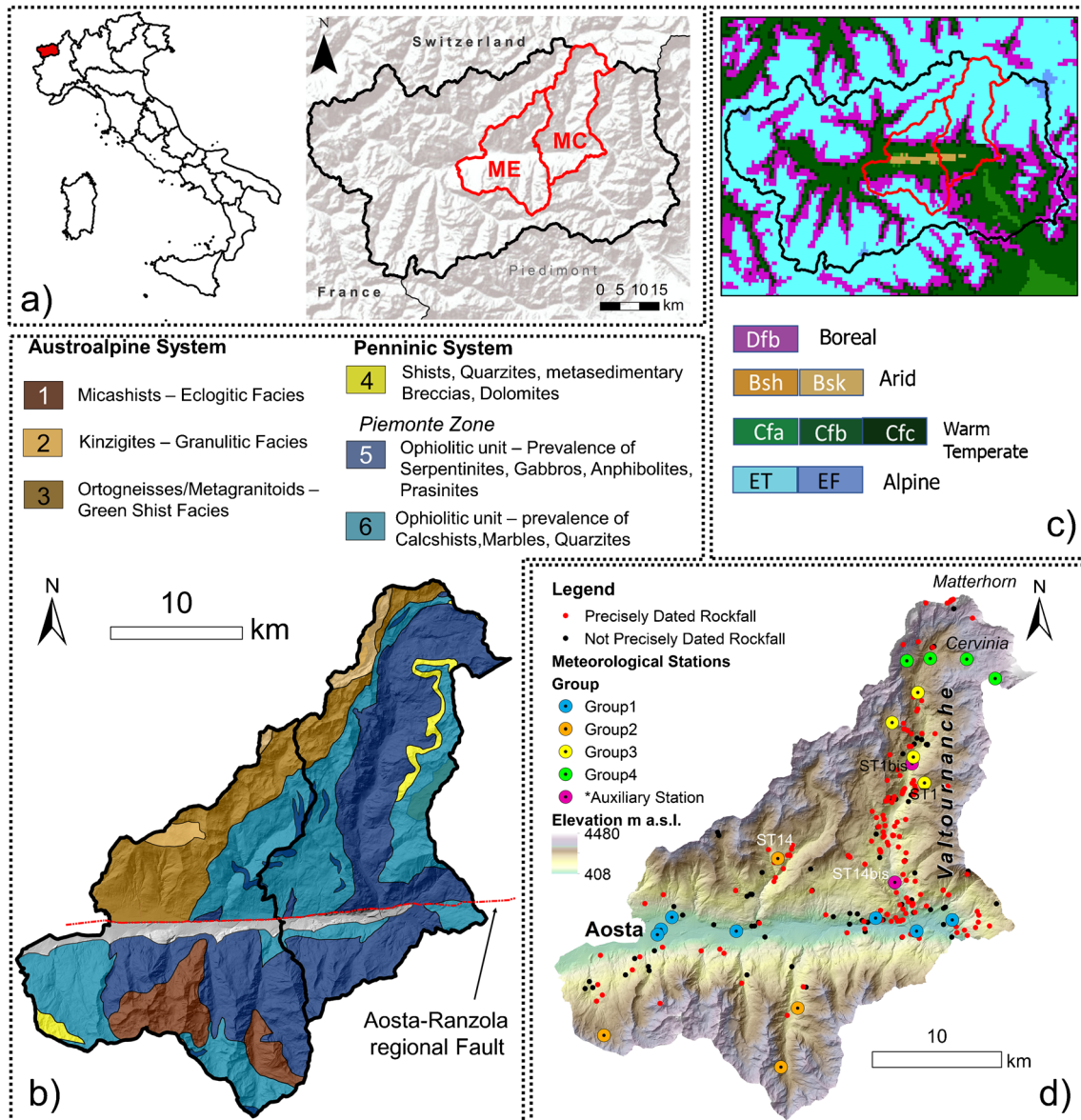
Fig. 1 **a** Aosta Valley and study area location (red borders). **b** Simplified geological map (modified from Bigi et al. 1990 and Ellero and Loprieno 2017). Geo-structural unit reference names: 1 Mont Emilius and Glacier Rafray units ME; 2 Valpelline unit V; 3 Cervin, Mont Mary and Pillonet units C-MM-P; 4 Pene Blanche and Pancherot-Cime Bianche units PCM; 5 Zermatt-Saas Oceanic unit Z (prevalence of serpentinites and metabasites); 6 Combin Oceanic unit C (prevalence of metasedimentary cover lithologies). **c** Aosta Valley Koppen's climatic classification (map available at http://koeppen-geiger.vu-wien.ac.at/alps.htm, Rubel et al. 2017). **d** Selected study area: rockfall and meteorological database location

cumulative distribution function (ECDF), which provided information on the probability of observing a rockfall of a certain volume.

Meteorological dataset and analysis

Meteorological stations and microclimate
A total of 19 meteorological stations are located within the study area (Fig. 1c). They record temperature (T), precipitation (P) and snow height (Hs) data with different temporal coverage and resolution. The stations are located at altitudes from 400 to 3000 m a.s.l. and in different microclimatic domains (i.e. different slope, aspect and

geomorphological-vegetational conditions). Starting in 2002, manual stations installed during the last century have been gradually dismissed and replaced by automatic ones (see Table 1 for details). Meteorological data are publicly available on the website of the Agenzia Regionale per la Protezione Ambientale (ARPA, http://www.arpa.vda.it/it/) and on the website of the Centro Funzionale Regione Autonoma Valle d'Aosta (https://cf.regione.vda.it/portale_dati.php). For nearby stations, the automatically and manually collected data series were joined to obtain longer representative time series, following suggestions of ARPA technicians. Two auxiliary manual stations (ST14bis-Promiod Covalou and ST1bis-Ussin in Fig. 1c), considered homogeneous and complementary to the automatic stations ST14 and ST1 for precipitation by ARPA

technicians, were also kept for rockfall-meteorological station association (refer to the "Rockfall and climate indices" section and Supplementary information for details). After merging, a further manual quality check was carried out, to find out residual anomalous values and gaps (especially zeros instead of missing values) in the data series.

The oldest data series dates back to 1980 (ST17); most of the manual stations were installed in 1990, whereas the automatic ones were installed in 2002. Manual stations present a daily temporal resolution, whereas the automatic ones collect data every 30 min. To join the data in order to carry out a comparative analysis of meteorological data, a Matlab R2019b® code to aggregate the sub-hourly data at the daily scale was developed. In some cases (namely ST2, ST13, ST16, ST7, ST9, ST10, ST11, ST12, ST28), not heated rain gauges were installed. Among these stations, those below 1500 m a.s.l. are characterized by missing data from December to March, while those located above 1500 m a.s.l. do not record from November to April. A synthesis of the available data is presented in Appendix Table 4. Once homogenized, an analysis of the daily aggregated T, P and Hs data was carried out to verify climate differences and similarities between stations. This step included the separation of the available meteorological stations in four groups, depending on location (E-W lineament, N-S lineament) and altitude range (Fig. 1c).

Group 1—Stations located along the E-W lineament (Aosta Valley) at an altitude range between 400 and 850 m a.s.l., ST2, ST3, ST4, ST13, ST16, ST17 and ST28.
Group 2—Stations located along the southern slope of the E-W main valley (Aosta Valley) at an altitude range between 1500 and 2300 m a.s.l., ST10, ST11 and ST12. Station ST14 was also added to this group with a comparative purpose, since it is the only station located at a comparable altitude but on the opposite flank.
Group 3—Stations located along the N-S lineament (Valtournenche Valley) at an altitude range between 1300 and 2000 m a.s.l., ST1, ST9, ST26 and ST27.
Group 4—Station located at the head of Valtournenche Valley, at an altitude range between 2000 and 3100 m a.s.l., ST5, ST6, ST7 and ST8.

Temperature and altitudinal temperature lapse rate (ATLR)

An altitudinal temperature lapse rate (ATLR) for the study area was evaluated on an annual base. As temperature data were available for all automatic stations only from 2010 to 2018, the ATLR was evaluated within this time period and considered valid for the entire reference period 1990–2018, following the concept of Climate Normals (World Meteorological Organization 2007). A global ATLR for the study area was evaluated using mean annual daily temperature for the 2010–2018 period. Moreover, the covariable slope aspect was tested in addition to altitude to evaluate possible model improvements. Different ATLRs for the E-W lineament (Aosta Valley) and for the N-S lineament (Valtournenche Valley) were tested (using data from stations in groups 1–2 and groups 3–4, respectively) in comparison to the global ATLR. To compare the different models, the performance indices R-squared (R²), adjusted R-squared (Adj-R², to compare models with a different number of covariables) and predicted R-squared (Pred-R², to avoid model overfitting) were calculated. These comparisons were carried out only when a performance value (p-value) <0.05 for the model was verified.

Effective water inputs

Different studies (e.g. Nishii et al. 2013; Crosta et al. 2014) point out that water supply deriving from snowfall can be quite relevant for the development of slope instability phenomena. A procedure to correct rainfall data in order to account for snowfall-deriving water inputs was thus implemented, with slightly different steps according to the station type. The different station types were identified based on temporal coverage, temporal resolution, instruments and available data (Table 1).

T temperature, Phg liquid precipitation derived from rainfall plus melted snow inside heated rain gauges, P rainfall from standard rain gauges, Hs snow height. ST9 belong to group B for data series between 1990 and 1998 and to group C for data series between 1998 and 2018

The correction was carried out at the daily resolution, despite the availability of sub-hourly data (i.e. 30 min) for most stations. This choice was made because the daily time step already allows considering the occurrence of melting, freezing and melting-refreezing processes—critical for snow melt contribution—by observing daily minimum and maximum temperature and their relationship with the 0 °C threshold. Further detail, such us including snow melting and refreezing processes at the hourly scale, was considered beyond the scope of this study. The correction procedure steps are described below.

Step 1 Identification of snowfall initiation representative temperature (Ts), degree day factor and average snow density from stations equipped with snow gauges and thermometers (i.e. type A and type D stations). For the definition of Ts, all positive temperature values corresponding to snowfall initiation were sampled (i.e. when the difference between Hs at day i and Hs at day $i-1$ is positive, $Hs_i - Hs_{i-1} > 0$ cm). A representative Ts was derived as the average of the sampled data. The calculated Ts value represents the temperature cut-off adopted to discriminate between solid (below Ts) and liquid (above Ts) precipitation in the subsequent steps. In the following, daily Hs data were converted into snow water equivalent (SWE) by using the classical equation (Seibert et al. 2015):

$$SWE = Hs\frac{\rho snow}{\rho water} \qquad (2)$$

where $\rho snow$ is snow density and $\rho water$ is water density. An average snow density value equal to 300 kg/m³ was attributed based on literature about snow properties in the Italian Alps (Pistocchi 2016; Guyennon et al. 2019). Water density was set at the commonly used 1000 kg/m³ value. Following DeWalle and Rango (2008), a mean degree day factor was calculated for the study area. According to this approach, the daily melt rate MR (mm/day), expressed as equivalent water depths, is given by:

$$MR = Cm*T_{mean} \qquad (3)$$

where T_{mean} is the mean daily temperature and Cm (mm/degree day C) is the degree day factor. At each station, to obtain daily Cm values, Eq. 3 was inverted setting MR equal to the previously calculated SWE (Eq. 2).

Table 1 Station types, depending on sensors and data availability

Station type	Sensors	Data	Station IDs
A	Heated rain gauge Snow gauge Thermometer	Phg, Hs, T	ST1, ST5, ST8, ST26, ST27, ST17, ST14
B	Heated rain gauge Thermometer	Phg, T	ST3, ST4, ST9 (1990–1998)
C	Rain gauge Thermometer	P, T	ST13, ST9 (1998–2018), ST16, ST10, ST28
D	Rain gauge Thermometer Snow gauge	P, T, Hs	ST7, ST11, ST12
E	Rain gauge	P	ST2
F	Thermometer	T	ST6

Step 2 Calculation of the actual daily liquid input (*Peff*) for type A and type B stations. Conceptually, the actual daily liquid input consists of the precipitation recorded at the heated rain gauge (*Phg*) deprived of the precipitation snow fraction (i.e. when $T_{mean}<Ts$) and with the addition of the snow melt from the accumulated snow (i.e. when $T_{mean}>0$ °C and *SWE*>0). Numerically, *Peff* was derived as follows:

$$Peff(i) = \begin{cases} 0, & Tmean \leq Ts \\ Phg(i) & Tmean > Ts \text{ and } SWEr(i-1) = 0 \\ MR(i), & Tmean > 0 \text{ and } Phg(i) + SWEr(i-1) > MR(i) \\ Phg(i) + SWEr(i-1), & Tmean > 0 \text{ and } Phg(i) + SWEr(i-1) \leq MR(i) \end{cases} \tag{4}$$

where *SWEr* is the corrected *SWE* amount deprived of the melted fraction of snow, or with the addition of the precipitation snow fraction, and it is updated daily as follows:

$$SWEr(i) = SWEr(i-1) + Phg(i) - Peff(i) \tag{5}$$

Step 3 Reconstruction of missing data (i.e. winter months data) for type C stations. It relayed on using a multiple regression procedure based on correlation of the type C stations available data with the closest type A and type B stations (i.e. one to three stations in a maximum radius of 9 km). A regression equation derived from the contemporary records was considered satisfactory for R-squared larger than 0.75. If this threshold was not reached, the type C station data were discarded. Once the time series were reconstructed, type C station data underwent the procedure described in Step 2.

Step 4 Conversion of snow gauge *Hs* data into *SWE* through Eq. (2) to obtain winter water inputs for type D stations. This procedure was carried out only for days in which a melting episode was recorded (i.e. $Hs_i - Hs_{i-1} < 0$).

Station ST2 is not equipped with a heated rain gauge (like group C stations) but was discarded from the procedure due to the completely lack of temperature data.

Rockfall and climate indices

Using the original and processed time series, relationships between dated (at least date of occurrence) rockfall events and climatic conditions were explored. Rockfall events were assigned a reference weather station based on two principles: (i) proximity, considered by using Thiessen polygons, and (ii) temporal coverage (i.e. meteorological data must be available on the day the rockfall event occurred and for the time windows relevant for the analysis). In case the two principles could not be mutually satisfied, the rockfall event was discarded from the analysis. Due to data availability (type, time coverage, time resolution), not all the four climate indices (STR, EWI, WD and FT, see Table 2 for definition) could be calculated at every station. Therefore, the configuration of the rockfall-station association and the number of stations and rockfalls included in the analysis resulted slightly different for each of the four indices (Table 2). For more details on the rockfall-station configuration and the Thiessen (Voronoi) polygons used, please refer to the Supplementary information.

Climate indices definition and calculation
Climatic conditions were defined in terms of four indices, which consider both short-term (up to 120 h) and long-term (up to 1 year) periods. The four indices are (i) STR, cumulated rainfall in 0.5-, 1-, 3-, 6-, 12-, 24-, 48-, 72-, 96- and 120-h periods (effect of short-term rainfall); (ii) EWI, daily, 3-, 7-, 15-, 30- and 60-day cumulated precipitation, including snow water inputs (effect of effective water inputs); (iii) WD, the number of wet and dry episodes in 30-, 60-, 120-, 180- and 365-day periods; and (iv) FT, the number of freeze-thaw cycles in 1-, 3-, 7-, 15-, 30-, 60-, 120, 180- and 365-day periods. Time series of each index were calculated at suitable stations from 1990 to 2018 (or for the available time period, if shorter) and summarized by means of statistical distributions. Not every station dataset covers the entire reference period 1990–2018, but based on the *Climate Normals* concept

Table 2 Rockfalls-stations schematic configuration depending on the climate index

Index	ID	No. of rockfalls (out of 168)	Temporal resolution	Starting parameter	Selected durations	Station IDs
Short-term rainfall	STR	96	30 min	P/Phg	0.5, 1, 3, 6, 12, 24, 48, 72, 96, 120 h	ST1, ST2, ST3, ST4, ST5, ST7, ST8, ST9, ST10, ST11, ST12, ST13, ST14, ST16, ST28
Effective water inputs	EWI	138	1 day	Peff	3, 7, 15, 30, 60 days	ST1, ST3, ST4, ST5, ST7, ST8, ST9, ST10, ST11, ST12, ST13, ST14, ST16, ST28, ST26, ST27
Wet and dry episodes	WD	95	30 min	P/Phg	30, 60, 120, 180 and 365 days	ST1, ST2, ST3, ST4, ST5, ST7, ST8, ST9, ST10, ST11, ST12, ST13, ST14, ST16, ST28
Freeze-thaw cycles	FT	117	30 min	T	1, 3, 7, 15, 30, 60, 120, 180 and 365 days	ST1, ST3, ST4, ST5, ST6, ST7, ST8, ST9, ST10, ST11, ST12, ST13, ST14, ST16, ST28

(World Meteorological Organization 2007), the statistical distribution analysed for each station is considered representative of the entire reference period even when shorter.

For the calculation of STR and EWI indices, a rolling sum was applied for each chosen duration. For the STR index, the rainfall data series at 30-min resolution (i.e. both for heated and not heated rain gauges) were used as input, while for the EWI index the corrected daily *Peff* data series were employed.

Wet and dry episodes are calculated with a temporal resolution of 30 min. A wet episode occurs when rainfall in 30 min is ≥0.2 mm (that is the detection limit of the available rain gauges), showing at least an increasing humidity in the area. A dry episode occurs when in 24 consecutive hours no precipitation is detected. These criteria were set considering the available definition of independent rainfall events at the slope (macro) scale (D'amato et al. 2016); albeit regarding intact rock specimens and not fractured rock masses, this interval is also included in the range of typical procedures at the laboratory (micro) scale, which includes several different drying intervals from 12 h to 7 days depending on rock type and drying temperature (Kegang et al. 2016; Yang et al. 2019 and references therein). The WD index is expected to have an influence on rock weathering and mechanical weakening after a consistent number of cycles, even on the single laboratory sample; to be able to observe an influence at the rock wall scale, it is reasonable to amplify the observation window in terms of time duration. Furthermore, to avoid a misleading superimposition of this index with the cumulated precipitation indices, the smaller duration investigated was 30 days.

The FT index was based on T data with a temporal resolution of 30 min. A cycle is defined as a temperature transition across 0 °C, in both directions (from positive to negative and to negative to positive). Available data refer to air temperature and not to rock temperature, which is not available for the area and very difficult to acquire with good spatial and temporal resolutions (Nigrelli et al. 2018). However, for each rockfall, the temperature data series of each reference station were extrapolated to the failure zone altitude by applying the ATLR (see the "Temperature and altitudinal temperature lapse rate (ATLR)" section). Therefore, for each rockfall scarp location, the related statistical distribution of the

index was produced applying ATLR to the data series of the associated station. Moreover, as for the wet and dry episodes, not ordinary conditions are expected to be more frequent in the longest time periods. Nevertheless, all the time windows used for the other indices were analysed to avoid neglecting the joint effect of freezing and thawing of water producing rock mass fatigue in shorter durations.

For WD and FT indices, a rolling sum technique was applied for each duration. To build their distributions, only records in correspondence of transitions in the number of cycles (episodes) were accounted (i.e. consecutive repetitions of the same number were disregarded). This computational scheme was adopted to avoid multiple counting of the same cycle (episode).

The distribution for the STR index was obtained by calculating cumulated rainfall for each duration and then summarized by monthly maxima boxplots; this choice is justified to account for rainfall seasonality as short-term events are considered for this index. For the EWI index, an empirical cumulative distribution function (ECDF) representation was preferred to summarize the statistical distribution related to each station, as it is a complete description of the sample (without a monthly distinction as durations involved transcend monthly subdivisions). For WD and FT indices, a boxplot representation was preferred to summarize the statistical distribution related to each station, as it is more suitable for discrete data as cycles.

Definition of not ordinary conditions

For each rockfall, the climate indices values associated with the triggering time of the event were extracted from the reference station time series. For the calculation of the STR index value at triggering time, when the date but not the hour of the rockfall event occurrence was known, the entire day dataset was considered (i.e. until 12 pm). Then, the highest cumulated value of the correspondent day of occurrence of each duration was associated with the event.

As the goal was to investigate the severity of the triggering conditions, index values at triggering were evaluated in relation with the correspondent index distribution calculated at the reference station or, alternatively, in comparison to a global reference

sample (see the "From indices to thresholds" section for additional details). The comparison was carried out for each considered durations (as the critical duration is not a priori known), and it was evaluated at which percentile of the distribution the index value associated to the event triggering time corresponded. This procedure aimed at identifying if rockfalls occurred during not ordinary conditions (i.e. in correspondence of high percentiles of the distribution) definable as possible triggering conditions if the associated duration is short, or as possible preparatory conditions (in terms of repeated stresses perpetuation) if the associated duration is longer.

For each climate index, the critical percentile to recognize a condition as not ordinary was defined as the value exceeded by at least the 50% of the rockfalls and corresponding at least to the 75th percentile but not over the 90th percentile of its distribution. These criteria were chosen for two reasons. First, the procedure aims at accounting not only for extreme events but also for severe ones, potentially neglected with too high percentile cut-offs (e.g. 95th or 99th, usually adopted for extreme events analysis; Camera et al. 2017). Second, considering 50% of the rockfall population for the recognition of the critical percentile should allow to include events occurred in severe (not extreme) conditions. Furthermore, if a consistent number of rockfall events (50% or more of those considered for each index) could be linked to specific climatic conditions, these conditions can be considered a reliable causation of the preparatory or triggering effect of climate on rockfalls.

From indices to thresholds

For those indices respecting the criteria of percentage of events and percentiles presented above ("Definition of not ordinary conditions" section), empirical thresholds (intensity-duration and number of cycles-duration thresholds) were defined. In case a specific rockfall presented index values higher than the critical percentile for more than one duration, the value closest to the critical percentile was considered and used for threshold construction. For the actual construction of the intensity-duration curve, the selected couples of values were interpolated using the nonlinear least square fit algorithm of the Matlab® Curve Fitting Toolbox™ to adhere to a power law function. In the following, shape and coefficient were adjusted by trial and error to define the most appropriate function so that the couples of values representing rockfall related to not ordinary conditions would fall above the resulting curves, except for some evident lower outliers.

These thresholds were constructed based on the previously defined critical percentiles exceedances in respect to the distribution associated to the single stations (i.e. "local approach"). However, when this type of intensity-duration (ID) thresholds are defined for a specific area, they cannot be easily exported to neighbouring regions due to meteorological and climate variability not included in the ID thresholds (Guzzetti et al. 2007). This is typically the case of mountain regions. Thus, to readjust data coming from different microclimatic conditions (e.g. valley bottoms and high peaks), two approaches were tested. First, a global approach was explored. Analogously to the local approach, the couples of values for threshold construction were selected by comparing rockfall-related indices values with the critical percentile value of the correspondent distribution, which in this case was built up using data coming from all the stations joined together.

This global threshold was considered reliable only if similar to the local approach based one. If the global threshold was not considered reliable (i.e. too influenced by specific stations characteristics), normalized thresholds were analysed. For the precipitation-related indices (STR, EWI), two types of normalization were carried out. The first threshold normalization was performed based on the mean annual precipitation (MAP), while the second normalization was based on the rainy day normal (RDN), which is the ratio of the MAP to the mean annual number of rainy days (Guzzetti et al. 2007, 2008; Peruccacci et al. 2017; Leonarduzzi and Molnar 2020). A normalized threshold was built also for the freeze-thaw cycles, taking inspiration particularly from the RDN normalization. It was defined as an intensity (of cycles)-duration threshold and introduced the freeze-thaw normal (FTN) normalization factor. Analogously to the RDN, the new freeze-thaw normal parameter is calculated as the ratio between the mean annual number of FT cycles and the mean annual number of across zero days (i.e. days where daily T_{max} is positive and T_{min} is negative). The threshold normalized to the FTN was thought to allow the comparison of rock walls at different elevations, which are exposed to different temperature regimes. Moreover, differently from normalizing only for the parameter mean annual freeze-thaw cycles (analogue to the MAP), it inherently accounts for whether the cycles are concentrated in some periods of the year or if they are homogeneously distributed throughout the year.

Exploring the role of positive temperature and gradients

Although of secondary importance in the Alpine context (see the "Introduction" section), the role of positive temperatures in thermal stress–induced fracturing and rockfall initiation is worth to be investigated. An exploratory analysis regarding high temperatures was set up for those rockfalls resulting not associated to any of the previous described indices. Indeed, summertime rockfalls that seem unrelated to any climatic triggering-preparatory factor could be explained with not ordinary positive temperatures and temperature gradients (Collins and Stock 2016). In particular, following a similar approach as for the other indices and according to findings of previous studies (Collins and Stock 2016; Collins et al. 2018), the number of days, before rockfall occurrence, in which maximum daily temperature (Tmax) was recorded above the 99th percentile of its complete distribution and above the 90th percentile of its July to August distribution was calculated. Furthermore, the number of days, before rockfall occurrence, in which the daily temperature gradient (ΔT) was recorded above the 90th percentile of its distribution was calculated. As for the previous indices, distributions were calculated with all the available data for the reference period 1990–2018 and in fixed time periods from 1 to 60 days.

Rockfall characteristics and relationships with climate indices

Besides threshold construction, by linking rockfalls to climatic indices, an analysis was carried out to recognize seasonal patterns in the role played by the different triggering and preparatory factors. The relationships between volume, altitude classes and climate were investigated, too. To have a more intuitive comparison between the different classes (of both volume and altitude) in case of large differences in the number of samples (rockfall events), the analysis was carried out in relative terms, normalizing each term to the total number of rockfalls in the class.

Finally, possible relationships of rockfall abundancy and climatic indices associations with the underlying geological unit or lithology were investigated. Six geological units (see Fig. 1b) were extracted from the structural model of Italy at the 1:50 000 scale (Bigi et al. 1990) and from Ellero and Loprieno (2017), while seven rock types were extracted from the geological map at the 1:10 000 scale of the Aosta Valley region (available upon request on the Aosta Valley Geoportal http://geologiavda.partout.it/cartaGeologicaRegionale?l=it). Rock types included (in order of areal abundancy) (i) serpentinites-prasinites; (ii) meta-granitoids; (iii) micashists and other metasedimentary shists; (iv) metabasites; (v) calcshists; (vi) marbles; (vii) dolomites; (viii) tectonized rocks; (ix) sedimentary breccias; and (x) quarzites.

Results

Rockfall database

For the reference period (1990–2018), 243 rockfall records were extracted from the Landslide Regional Database and validated. Almost 70% of the records (168 out of 243) come with the exact date of occurrence, whereas the remaining 30% (75 records) have only the month and year or only the year of occurrence.

Although the temporal distribution of the events in the study area (Fig. 2a) seems to suggest a slight increase in rockfall frequency in recent years (since 2000), such evidence could be linked to a reporting bias, following the establishment of more sophisticated monitoring networks and technologies. This issue was already pointed out by several authors working on Alpine rockfalls (Nigrelli et al. 2018 and reference therein), and inventory bias is a common and known problem when dealing with such natural hazards (Guzzetti et al. 2012; Petschko et al. 2016; Steger et al. 2016).

The seasonal characterization of rockfall occurrence (Fig. 2b) showed an almost bimodal distribution of the events. The highest peak is recorded in spring (March, April and May), and a secondary peak is observed between October and January, with a slight decrease in December.

Only 199 rockfalls have an associated volume information, which in some cases is only a magnitude order and not a precise value. The most frequent volume class resulted to be 5–50 m^3 (Fig. 3a); according to the data available in the inventory, the probability of occurrence of a rockfall with a volume larger than 10 m^3 is about 0.35, whereas the probability to observe a rockfall with a volume higher than 100 m^3 is of 0.15 (Fig. 3b).

In terms of altitudinal distribution (Fig. 3c), events appear to concentrate along the mid altitude range (400–2000 m a.s.l.). This relative high abundance of rockfalls at these altitudes can be explained with the difficulties in monitoring high mountain environments, unless characterized by human activities (e.g. ski resorts, hiking itineraries). As a demonstration, in the area around Matterhorn—famous for hiking trails, climbing and the ski resorts of Cervinia and Zermatt—dated events are available even at very high altitudes (>3200 m a.s.l.).

Meteorological dataset and analysis

The preliminary analysis confirmed that, despite general similarities between stations at comparable altitudes, there is a significant climatic variability within the study area. Local orographic-geomorphological dynamics seem important to determine differences in the rainfall and snowfall amounts, even between nearby stations. At high elevations, the northern head of Valtournenche Valley (station group 4—see the "Meteorological stations and microclimate" section and Fig. 1) resulted to be particularly rainy (average annual precipitation 963 mm) with peaks mostly in May, August and November and with snow intakes (average annual snowfall 694 cm) larger than those recorded on the southern slopes of the E-W lineament of Aosta (station group 2, average annual rainfall 774 mm with peaks in May and September-October-November and average annual snowfall 486 cm). Comparing the east and the west part of the study area, the former (Mont Cervin area, average annual rainfall 811 m) resulted to be more humid than the latter (Mont Emilius, area average annual rainfall 671 m). In general, at low-middle elevations along the E-W lineament (i.e. group 1 stations), rainfall peaks are uniformly reached in spring and autumn (especially May and November).

Global and E-W lineament ATLRs, evaluated with only the altitude covariable, resulted to have good model performance indices (Table 3). The global ATLR was −0.53°C/100 m and the same ATLR was obtained for the E-W lineament. Conversely, the ATLR for the N-S lineament resulted to be smaller (−0.43°C/100 m) but with a lower predictive performance (i.e. lower Pred-R^2, see Table 3). The slope aspect covariable resulted to added noise to the global and E-W lineament ATLRs (i.e. lower Pred-R^2) but improved slightly to the N-S lineament ATLR. The mean annual global ATLR resulted to be the most reliable as it shows the highest regression predictive index (Pred-R^2) and it agrees with the values traditionally recorded in the Alpine region (Rolland 2003).

Regarding the effective precipitation calculation procedure, average *Ts* for single stations ranges between 1.8 and 2.8 °C, whereas the median *Ts* ranges from 1.4 to 2.4 °C. A *Ts* value equal to 2°C was thus chosen for the entire study area. For the degree day factor *Cm*, the mean value of the stations' medians (i.e. 3.5 mm/degree day C) was selected as representative for the study area. Among the type C stations, only station ST9 was discarded in Step 3 (i.e. reconstruction of winter data series by means of multiple regression) because the implemented regression model did not reach the set criteria, with a R-squared equal to 0.66 (< 0.75). Due to these scarce results, no correction is thus carried out for data from 1998 to 2018. However, the station was not discarded for further analysis on the EWI index—rockfalls correlation. Firstly, ST9 almost unique position at the bottom of the middle Valtournenche Valley was considered crucial for the comparative analysis. Secondly, data from 1990 to 1998, coming from the old manual ST9 station, were suitable for snow melting inputs correction (i.e. type B station). Moreover, the majority of the rockfalls associated to ST9 from 2000 to 2018 (i.e. 6 out of 8) occurred in summer and autumn, thus without the strict necessity of snow melting inputs reconstruction. However, for this station the possibility of slightly underestimated ECDFs has to be considered in performing the consequent comparative analysis.

Rockfalls and climate indices

Short-term rainfall

As a representative example, Fig. 4 compares, for station ST3, the maximum cumulated rainfall values in the different selected duration (i.e. 0.5 to 120 h) before each rockfall event (if available,
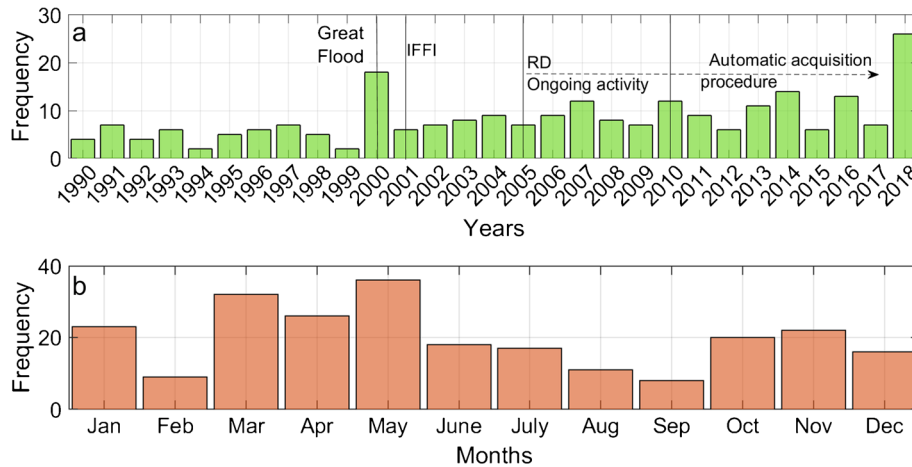
Fig. 2 a Annual frequency of rockfalls in the study area and historical evolution of the regional database (RD); **b** monthly frequency of rockfalls in the study area

corresponding to the exact hour of occurrence, alternatively to the daily maximum) with the distribution of the monthly maxima cumulated values in the same duration and for the entire reference period. It shows that only 16 rockfall events (i.e. 17%) were associated to the exceedance of the 75th percentile of the distribution of at least one duration.

These results highlight that, except for some rockfalls associated to extreme events (such as heavy summer storms), in most cases short rainfall events alone are not able to justify the occurrence of rockfall events. Therefore, in the study area and for the considered volume range (more than 5 m³), a direct cause-effect relationship between rockfalls and short rainfall events cannot be assumed. This index, as it did not respect the procedure requirements adopted, was discarded.
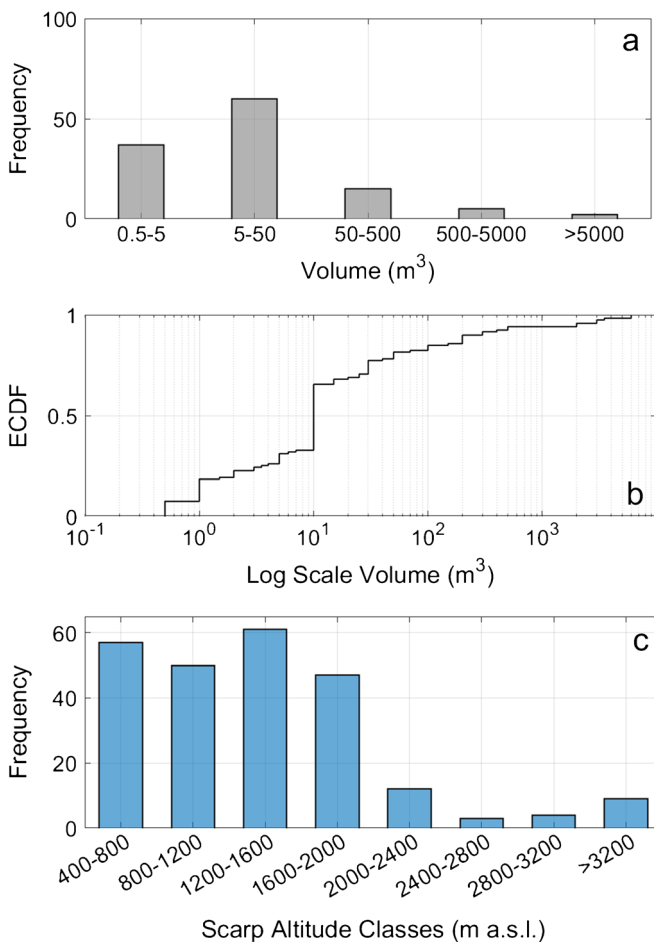
Effective water inputs

As a representative example, Fig. 5 shows the ECDF ensemble for station ST14, representing the distribution of the EWI index for the different chosen durations (i.e. 1 to 60 days) and the associated rockfall values. Although the short-term rainfall index was discarded, by introducing durations of 1, 3 and 7 days in the EWI index, short and intense events were considered in the threshold construction, too. Carrying out the comparison with the ECDF curve, it resulted that more than 50% of the rockfalls were associated to at least one value larger than that corresponding to the 0.9 probability of the ECDF curve. This defined the 90th percentile as that representing not ordinary conditions for the area. More precisely, 73 rockfalls out of 138 were associated to not ordinary conditions. By considering the 75th percentile, the exceedance would increase to 80 rockfalls, leading to an increase in the relative number of rockfalls characterized by not ordinary conditions from 52.9 to 58.0%. However, the 90th percentile satisfies stricter criteria and it is therefore preferred.

The global approach was evaluated, too. Consistently with the local station approach, it shows more than 50% of the rockfalls associated to a value over 0.9 of the global ECDF curves, confirming the robustness of the adopted method. However, the global 0.9 cumulated rainfall values resulted to be very similar to those obtained for the stations with the longer temporal coverages, mostly located in the Mont Cervin subarea (7 out of 9 stations). In particular, adopting a global approach resulted in having (+3) events in not ordinary conditions in the northern part of

Fig. 3 a Frequency histogram of rockfall volume classes. **b** Empirical cumulative distribution function (ECDF) of rockfall volumes. **c** Rockfall frequency vs scarp altitude

Table 3 R-squared (R^2), adjusted R-squared (Adj-R^2) and predicted R-squared (Pred-R^2) values for the tested annual ATLR

		Global		E-W lineament		N-S lineament	
Altitude	R^2	0.969	R^2	0.964	R^2	0.938
	Adj-R^2	0.967	Adj-R^2	0.959	Adj-R^2	0.922
	Pred-R^2	0.960	Pred-R^2	0.949	Pred-R^2	0.75
Altitude + aspect	R^2	0.973	R^2	0.964	R^2	0.978
	Adj-R^2	0.969	Adj-R^2	0.953	Adj-R^2	0.963
	Pred-R^2	0.957	Pred-R^2	0.900	Pred-R^2	0.81

Valtournenche Valley and (+5) in ordinary condition in its lower part. These resulting unbalanced relationships indicated a higher influence of data series of some stations in comparison to others in defining not ordinary conditions and consequently in threshold definition. This led to prefer the local approach and consequent threshold normalization (see the "From indices to thresholds" section). Therefore, MAP and RDN normalized thresholds based on the local approach were calculated and evaluated in comparison to the not normalized one (Fig. 6).

All the three thresholds are characterized by a negative power law. Figure 6 also shows that for very short (1 day) and very long durations ($\geq$ 30 days), the not normalized threshold has a lower capability than the normalized thresholds to discern between ordinary and not ordinary conditions. Over the threshold (Fig. 6a), it is possible to distinguish the overlap of couples of I-D values characterized by percentiles either larger or lower than 0.9. This means that the normalized thresholds are more reliable than the not normalized one since they smooth better microclimatic differences.

Wet and dry cycles

Wet and dry episodes were calculated with data covering the period 2002–2018 at almost every station and a temporal resolution of 30 min. No correction with snowfall data was adopted for this index; therefore, a bias due to not heated rain gauges (9 out 15 stations used for the index) has to be considered for further applications beyond threshold construction.

As a representative example, Fig. 7 shows the boxplot ensemble related to the wet and dry episodes distribution (durations from 30 to 365 days) with the associated rockfall occurrence values, for station ST1. Carrying out this comparison for each station and associated rockfalls, it resulted that more than 50% of the rockfalls (69 out of 95, 72%) were associated to at least one value over the 75th percentile of the distribution, thus defining not ordinary conditions for the area. By considering the 80th percentile, the exceedance would decrease to 44% (42 rockfalls), while considering the 90th percentile the exceedance would decrease to 17% (16 rockfalls).

The threshold construction was thus carried out. Conversely to the EWI index, the global approach seems applicable as the two thresholds resulted to be very similar (Fig. 8). Moreover the 75th global percentiles resulted to be very close to the median value of the 75th stations associated values distribution (boxplots in Fig. 8). The global threshold is almost correspondent to the threshold built with the classical station by station approach. This does not state that the number of wet and dry episodes is the same within the area, but only that number of episodes related to not ordinary

conditions leading to rockfall phenomena is quite similar for the rock masses in the area. As a global threshold for the whole area was individuated for this index, no further normalizations were carried out. The threshold curves have the form of a positive power law.

Freeze-thaw cycles

Figure 9 shows, as an example, the boxplots ensemble of the freeze-thaw cycles distribution (duration from 30 to 365 days) and the associated rockfall occurrence values, for station ST8. Carrying out this comparison for each station and associated rockfalls, it resulted that more than 50% (64 out of 117, 55%) of the rockfalls were associated to at least one value over the 75th percentile of the distribution, thus defining not ordinary conditions for the area. Considering the 80th percentile the exceedance would decrease to 47.8% (56 rockfalls), while selecting the 90th percentile the exceedance would drop to 43.5% (51 rockfalls).

Figure 10 displays the two thresholds built for the FT index. The first relates the number of FT cycles (NoC) and duration, and it was built from the original station data (Fig. 10a); it has the form of a positive power law. The second threshold relates the intensity of the FT cycles, normalized to the FTN parameter (I_{FTN}), to the duration (Fig. 10b). Coherently with the use of intensities instead of number of cycles, the resulting curve has the form of a negative power law. A global threshold in this case was not considered because it would have given much more weight to the highest elevations, hiding not ordinary conditions exceedance for low-mid altitude rock walls. Temperature, differently from rainfall, is a continuous parameter, and rockfalls are an expression of the loss of equilibrium between rock masses and the external environment, including the oscillation frequency through 0°C. For these reasons, the most suitable approach seemed to be a normalization, which should highlight anomalous oscillation frequencies for specific local conditions. However, even the normalization was not able to capture entirely the extreme local variability of the phenomenon of freeze-thaw cycles.

As shown in Fig. 10, some rockfalls are evidently very distant from the threshold curve, both up and down; this means that the threshold could both underestimate and overestimate the process. A slight improvement with the normalized threshold could be observed for middle-long durations (i.e. 120 and 90 days), but a high dispersion persisted for the shortest and longest durations (i.e. 1 and 365 days). For the sake of completeness, the threshold normalized to the mean annual number of freeze-thaw cycles resulted to be more dispersed than the other two and can be found in the Supplementary information.
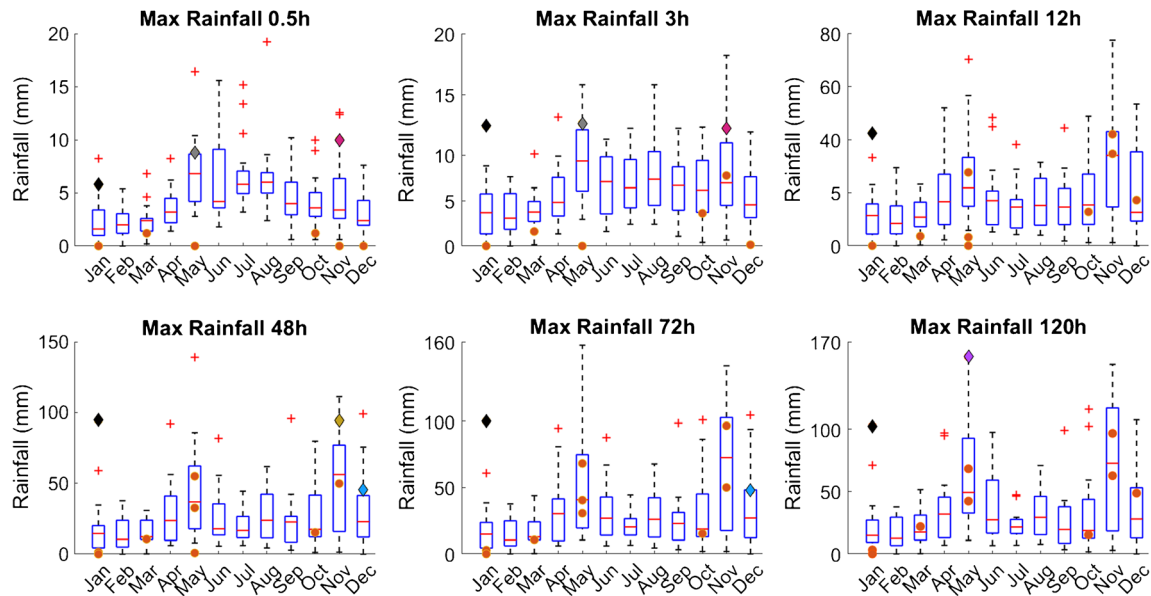
Fig. 4 Boxplots of monthly maxima cumulated rainfall for selected duration from 0.5 to 120 h. Points represent cumulated rainfall values corresponding to each rockfall event not exceeding the 75th percentile, while diamonds represent cumulated rainfall values corresponding to each rockfall event exceeding the 75th percentile (each colour represents a specific rockfall and is maintained between the boxplots). All the presented graphs refer to ST3 data and associated rockfalls as an explicative example. The bottom and top of each box are the 25th and 75th percentiles, the line in the middle of each box is the median, and outliers (crosses) are values whose distance from the box is higher than 1.5 times the interquartile range. Whiskers go from the end of the interquartile range to the furthest observation within 1.5 times the interquartile range

Deciphering triggering and preparatory climatic factors

Out of the 168 dated events, 136 could be linked to climate indices. The remaining 32 rockfalls were discarded due to the lack of complete climate data (e.g. missing data in the time window related to the index calculation). Among these 136 rockfall, more than 95% (130) resulted to be associated to not ordinary conditions of effective water inputs, wet and dry episodes, freeze-thaw cycles or to a combination of these factors. Only six rockfalls occurred during ordinary meteorological conditions for EWI, WD and FT indices. However, five of these occurred during summer and one
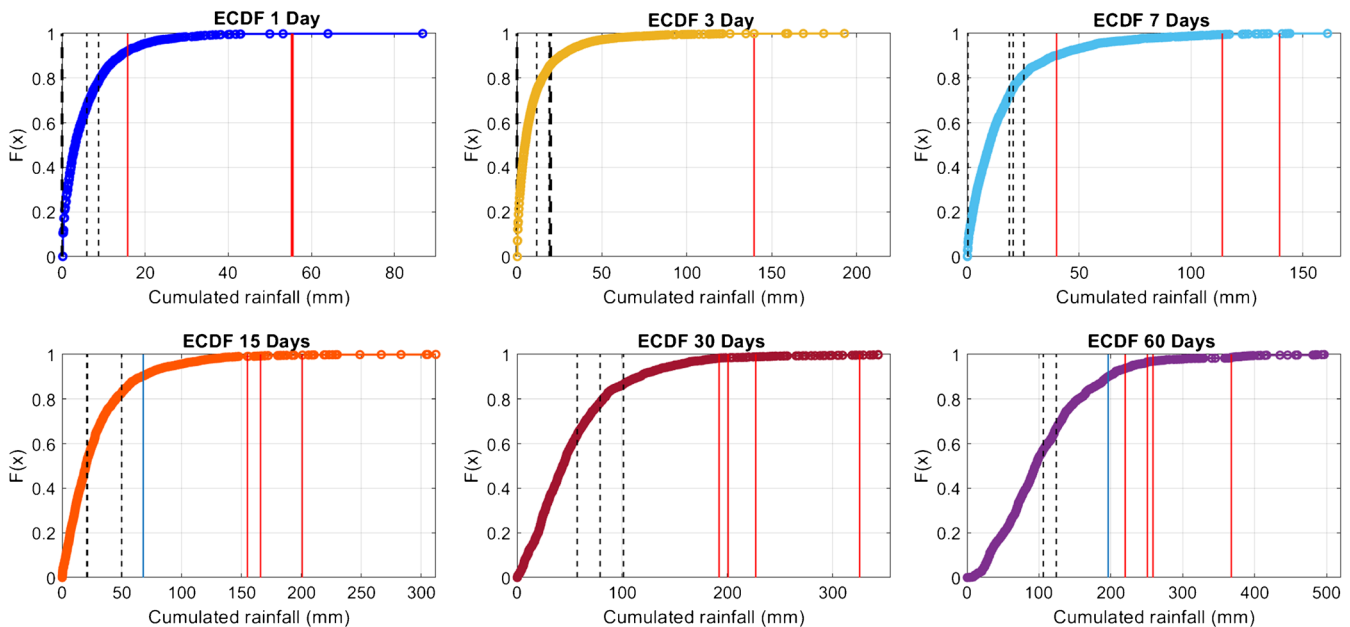
Fig. 5 ECDF curves of cumulated precipitation for duration from 1 to 60 days. Red lines represent rockfalls with cumulated rainfall values over the 0.9 probability for more than one duration; blue lines represent rockfalls with cumulated rainfall values over the 0.9 probability for a single duration; dotted black lines represent rockfalls with cumulated rainfall values never exceeding the 0.9 probability value. The presented graphs refer to ST14 data and associated rockfalls
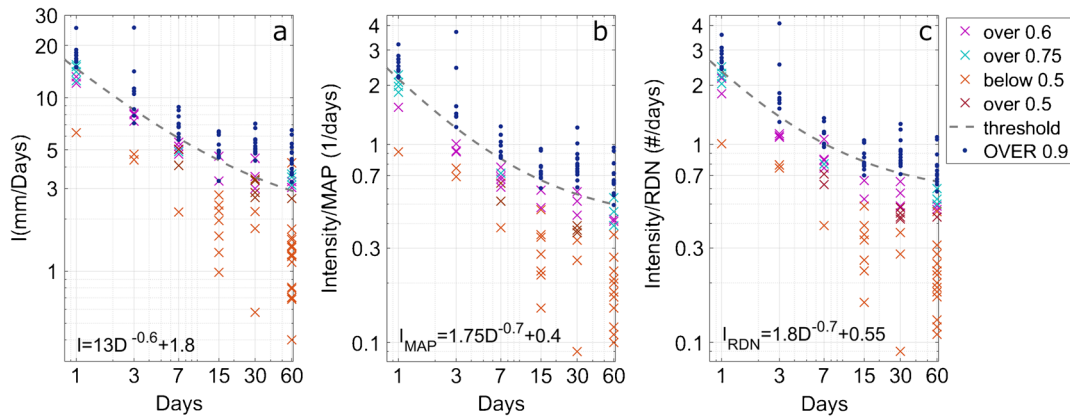
Fig. 6 Intensity-duration thresholds for the effective water input index. **a** Standard threshold. **b** Mean annual precipitation (MAP)-normalized threshold. **c** Rainy day normal (RDN)-normalized threshold

in early autumn, so their possible relation with positive temperature anomalies was analysed (Fig. 11). In particular, a rockfall that occurred in July 2017 at 1175 m a.sl. and a second one that initiated in August 2003 at 3735 m a.s.l. showed a high number of days, in different durations before their occurrence, in which daily Tmax was above the 99th percentile of the complete Tmax distribution or above the 90th percentile of the July to August Tmax distribution. Also, they showed a quite large number of days in which the daily ΔTs were over the 90th percentile of their distribution, together with another rockfall occurred on June 05, 2006, at 1850 m a.s.l. For the other three rockfalls—which took place at medium altitudes on August 05, 2016, July 01, 2006, and October 14, 2018, respectively—an influence of high temperatures and gradients was more questionable, even if they showed an increment of the number of days in which the daily gradient was above the 90th percentile in periods of 30 days and 60 days before their occurrence.
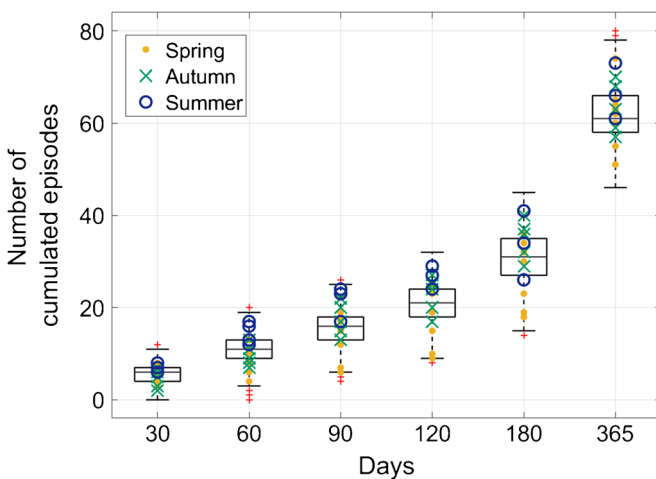
Figure 12 analyses the seasonality of the triggering and preparatory factors. It shows that:

(i)   During the spring season, the most frequent factor is made up of a combination of precipitation characteristics (EWI and WD indices) and FT cycles, followed by FT alone and EWI (or EWI combined with WD episodes). In spring, FT cycles could be linked, alone or in combination with rainfall, to 70% of the rockfall, stressing their predominant role in influencing the occurrence of such phenomena.

(ii) During summer, the combination of a precipitation-related index and FT cycles is still the most frequent association of factors leading to failure, reasonably due to the lag between stabilization of T above 0°C and snow melt water inputs still active at high altitudes. However, also WD cycles and effective precipitation have a high frequency. Some rockfalls could also be associated with high temperature peaks Fig. 11.

(iii) During autumn, precipitation is reasonably the main triggering-preparatory factor for rockfalls in the area, in correspondence with the second annual peak of the bimodal distribution of rainfall.

(iv) During winter months, a prevalent factor is not easily recognizable. However, effective precipitation seems crucial, especially in terms of snowfall income subject to intermittent accumulation and melting phases, or in combination with FT cycles, thus with freezing, melting and refreezing process.

This analysis also highlighted that the choice of the 75th percentile minimum cut-off to consider not ordinary conditions occurrence resulted suitable, as it was reached and exceeded throughout the year with different frequencies according to seasonality. As considered durations include both short-term (i.e. 1, 3, 7 days) and medium- to long-term (i.e. from 15 to 365 days) time periods, the seasonality of climate-related rockfalls can be biased depending on the duration considered critical. Nevertheless, this is consistent with the attempt to consider climate not only as a trigger but also as a long-term preparatory factor, going beyond the single season.

Relating rockfall scarps altitude and associated climate factors (Fig. 13a), a decreasing influence of EWI index could be observed by
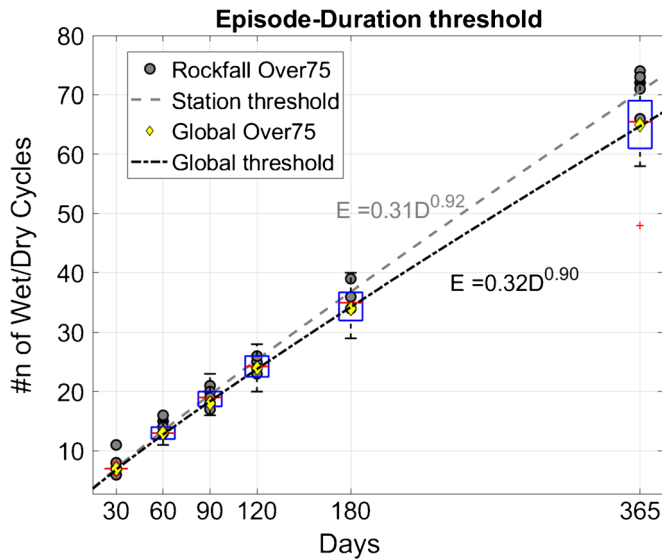

Fig. 7 Boxplots representing the statistical distribution of wet and dry episodes for duration from 30 to 365 days. Superimposed symbols represent rockfalls associated values, divided by season of occurrence. Figure refers to ST1 data and associated rockfalls. Boxplot statistical limits as in Fig. 4

Fig. 8 Episode-duration threshold for number of cumulated wet-dry episodes (30 to 365 days). Comparison between global and local (station-by-station) approach. Boxplots represent the 75th percentile distribution among the stations. Boxplot statistical limits as in Fig. 4

increasing altitude. Cumulated precipitation seems to be a very frequent triggering-preparatory factor at low-medium altitudes (400–1300 m a.s.l.). Conversely, WD episodes show a slightly growing effect on rockfall failure with increasing altitude. This could be linked to the different nature of precipitation events at high altitudes, where short and local storms prevail over high amounts of water resulting from long events. The association of FT cycles with EWI and WD episodes seems to remain stable with altitude. Finally, the single effect of FT cycles shows a peak at medium-high altitudes (1300–1800 m a.s.l.); this could be related to the transition zone where the 0°C temperature line is oscillating the most during the year.

Regarding the relationship between volumes and climate factors, only 73 out of the 136 analysed rockfalls have volume classes available;
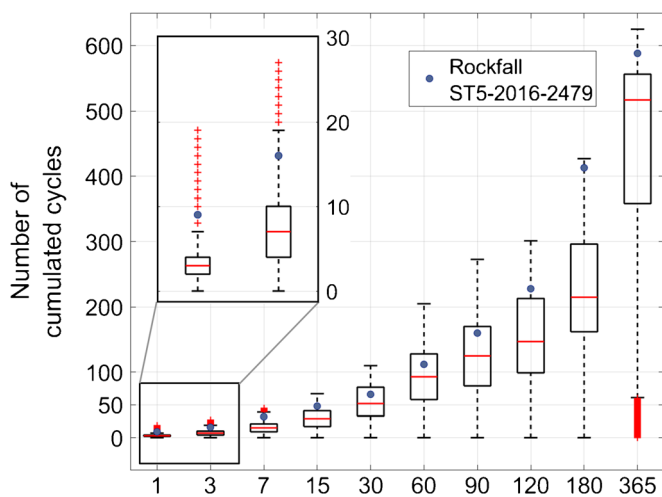
Fig. 9 Boxplots representing the statistical distribution of freeze-thaw cycles for variable durations. Black dots represent the rockfall associated number of cycles. Example from rockfall ST8-2016-2479 (i.e. rockfall related to station ST8, occurred in 2016 with a scarp located at 2479 m a.s.l.). Boxplot statistical limits as in Fig. 4.

therefore, only a partial analysis could be carried out (Fig. 13b). The WD episodes effect is most evident for the smallest rockfalls (0.5–50 m³). FT cycles alone and in association with precipitation-related indices are predominant for rockfalls of medium and high volumes (larger than 5 m³). EWI resulted to have a quite high effect both on small- and medium-sized rockfalls. However, more data on volumes are needed to reliably investigate these relationships.

By comparing rockfall abundancy with geological units (Fig. 14a), it resulted that the two most abundant units, the oceanic Zermatt-Saas and Combin units (38% and 33.8% of the study area respectively), gather the majority of rockfalls of the study area. This evidence is nonetheless confirmed in absolute terms of numbers of events per unit area (dots in Fig. 14a). Considering climatic factors (Fig. 14b), in the Zermatt-Saas unit, the most abundant triggering-predisposing factors were represented by rainfall (EWI or EWI+WD), followed by FT+EWI/WD. In the Combin unit, the opposite occurs. Only 10 rockfalls were recorded in the C-MM-P unit, covering 17.3% of the study area, and for this reason an assumption on the prevalent climatic indices is hardly feasible; however, 4 out of 10 rockfalls are ascribable to WD alone. The other three units are less abundant and with none or just 1 rockfall recorded.

Considering lithologies rather than units (Fig. 14c), it resulted that the number of rockfalls in granitoids is much less than in serpentinites-prasinites, having these two lithologies almost the same abundancy (24.7% and 23.3%, respectively) in the study area. In terms of number of events per unit area, metabasites and calcshists showed the highest value. Analysing the role played by climate (Fig. 14d), for serpentinites-prasinites lithology, the most common influencing factor was represented by the association FT+EWI/WD, followed by EWI or EWI/WD. Calcshists lithology was mostly associated to rainfall (EWI or EWI/WD), which doubled the FT+EWI/WD combination: For metabasites EWI or EWI/WD and FT+EWI/WD had almost the same abundancy. FT alone had almost the same abundancy among the three above-mentioned lithologies (slightly lower in serpentinites-prasinites). Although in granitoids and shists rockfalls are few and strong conclusions cannot be drawn, the events showed predominant relationships with WD and FT+EWI/WD, respectively.

The association between climatic indices and underlying geological units and lithologies should be linked also to local rock mass properties such as in situ stress and fracture network characteristics. Such an analysis would allow much more robust generalizations and the extrapolation of clearer relationships.

Discussion

This work explores four climatic indices as possible triggering and preparatory factors for rockfall instabilities in a sub-area of the Aosta Valley region, both considering short-term and long-term durations. Gunzburger et al. (2005) outlined that the distinction between triggering and preparatory factors, defined in terms of their action time frame, should not be intended as an absolute dichotomy, as they act in a continuous transition. This concept seems to be confirmed by the present work, as several rockfalls resulted to be associated to more than one duration corresponding to not ordinary conditions, and to a combination of different climatic indices acting at different temporal scales. In such cases it is almost impossible to state which condition (long-term index or short-term index) was responsible for final collapse. However, the definition of not ordinary conditions and the identification of indices critical combinations and thresholds can lead to a better
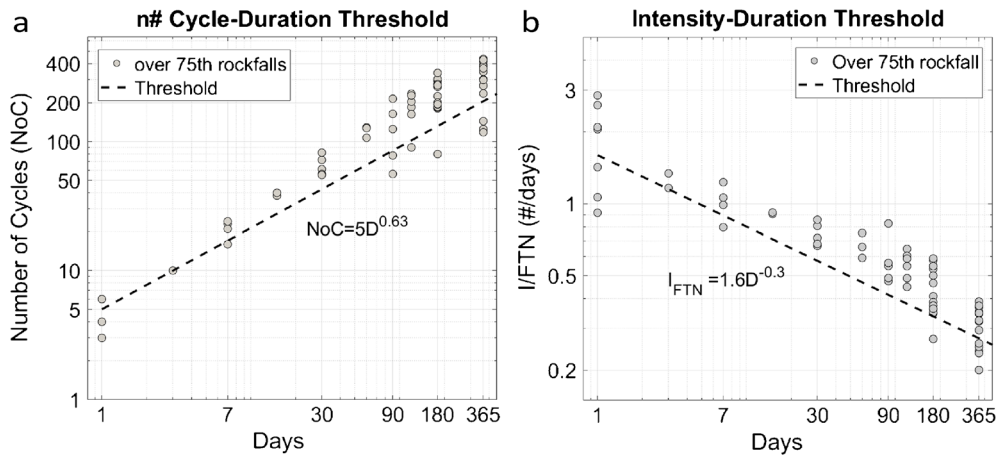
Fig. 10 FT Cycles-duration thresholds. **a** Standard threshold, log scale. **b** FTN-normalized threshold log scale

understanding of the mechanism of such events, helping in defining the most critical situations.

The historical rockfall inventory of Aosta Valley region was crucial for the whole analysis. The usefulness of not neglecting to record date and time of each rockfall event when known is indeed confirmed and could allow the calculation of specific climatic indices and thresholds.

However, although rich and suitable for the study, the analysis made on the location of source areas suggested a negative bias in event record acquisitions at high, poorly frequented elevations. This is a common and widespread problem, which leads to an incomplete (to an unknown extent) inventory (e.g. Petschko et al. 2014).

Fig. 11 Number of days before rockfall occurrence, in durations from 1 to 60 days, in which Tmax were above the 99th percentile ($Tmax\ 99^{th}$ if the distribution was built with all the daily Tmax values) or the 90th percentile ($Tmax\ (JA)\ 90^{th}$ if only based on July and August) and daily gradients was above the 90th percentile ($DeltaT\ 90^{th}$). Legend reports date of occurrence (dd/mm/yyyy) and altitude (m a.s.l.) in parentheses

The highest rockfall frequency occurred in spring (March to May) and a secondary one in winter, with its main peak in January. Macciotta et al. (2015) found a comparable peak in January, explained by freeze-thaw cycle occurrence. Frayssines and Hantz (2006) found a similar annual cycle for rockfall occurrence in the Grenoble area but with the primary peak in winter rather than spring. Compared to this study, the authors focused on larger rockfall volumes (mainly > 50 m³) and lower altitudes (from 200 to 2000 m a.s.l.); thus, they investigated events characterized by a lower occurrence of freeze-thaw cycles in spring.

The comparison between climatic conditions recorded before each rockfall occurrence and ordinary (i.e. typical) climatic conditions for the area follows the approach of Paranunzio et al. (2015). Differently from these authors, in this study the cumulated precipitation index was designed to include the water inputs coming from snow melting processes, and it was renamed as effective water input index. In addition, other processed indices were explored, namely wet and dry episodes and freeze-thaw cycles. Conversely to D'Amato et al. (2016), who found that short-term rainfall gives the higher rockfall frequency, the occurrence of not ordinary conditions for the STR index showed poor correlation with rockfall occurrence. This difference may be explained by the lower volume range studied by D'Amato et al. (2016), which is mainly below 1 m³. In the Canadian Cordillera, Macciotta et al. (2017) suggested that snow melt can explain a peak in rockfall record in February to March. Accounting for snow melting inputs was possible by developing a simple method based on degree day factor and snow data conversion. The obtained representative degree day factor of 3.5 mm C⁻¹ day⁻¹ resulted to be coherent with typical literature values, which range from 1.6 to 6.0 mm C⁻¹ day⁻¹ (USDA-NEH 2004; He et al. 2014). The adopted correction method obviously introduced some simplifications regarding the complex dynamic of snow-related processes. However, the results obtained demonstrated the primary importance and utility of snow-derived water inputs when investigating reasons for rock mass instabilities. Therefore, in agreement with findings of several authors (e.g. Nishii et al. 2013; Crosta et al. 2014), the results of this study strengthen the need for in-depth research on this topic.

Deriving thresholds, when the critical percentile was exceeded for more than one duration, the lowest value was used for threshold construction. This choice represents a conservative approach, which is reasonably preferable when dealing with natural hazards. In addition,
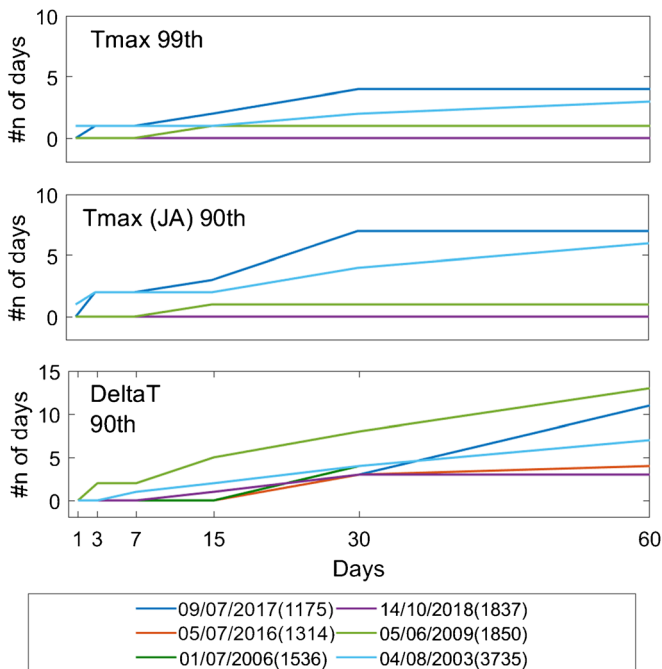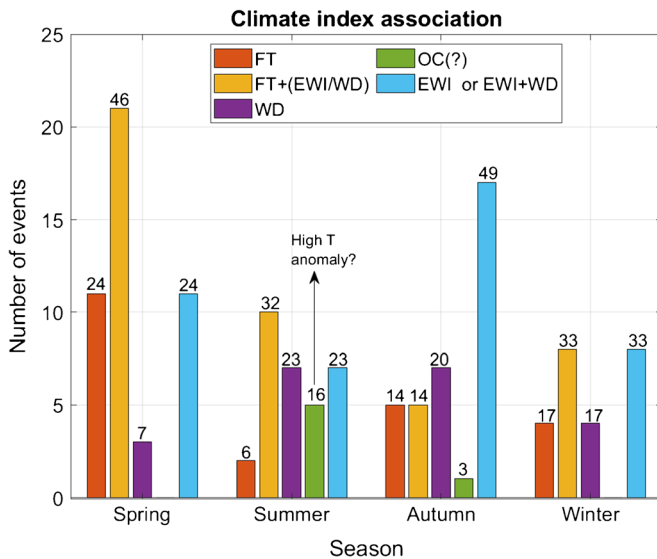
Fig. 12 Bar chart representing triggering and preparatory indices seasonal frequency. FT, freeze-thaw cycles; EWI, effective water inputs; WD, wet and dry cycles; OC, ordinary conditions. Numbers refer to the relative percentage of events of each season

the lowest critical value could correspond to residual geomechanical conditions, and therefore it could take into account the possibility of rockfall occurrence as secondary reactivations (i.e. linked to less intense triggers/preparatory factors). The lower dispersion obtained with normalized thresholds in comparison to those derived from the simple intensity-duration formulation confirms the utility of this approach in areas characterized by the juxtaposition of different climate types. This result agrees with findings of numerous previous studies (Guzzetti et al. 2007, 2008; Peruccacci et al. 2017; Leonarduzzi and Molnar 2020).

Despite the adoption of a normalization approach, the FT threshold construction was difficult due to high dispersion of the input data. Indeed, not ordinary conditions in term of freeze-thaw cycles can be very different depending on altitude, also considering that T is a continuous parameter and rockfalls can be the expression of the loss of the equilibrium between the rock mass system and the external thermal conditions. In this study, the temperature variability with altitude was implemented in the analysis by adopting an annual ATLR of −0.53°C/100 m, which is coherent with the annual lapse rates ranging from −0.54 to −0.58°C/100 m typical for various mountain regions in France and Italy (Rolland 2003). As shown by Nigrelli et al. (2018) and Kirchner et al. (2013), the application of a monthly or sub-daily ATLR could guarantee a detailed representation of temperature variation dynamics (temperature inversion phenomena, aspect and slope influence, vegetation and snow cover indirect effect through incoming solar radiation) and possibly an improved modelling of FT cycles. However, it should be considered that the final aim of this study is not to analyse a particular rockfall or meteorological event but to produce an overall analysis of the influence of different climate indices on rockfall occurrence and to develop thresholds extendable on a sub-regional scale. Thus, the annual (generally accepted) ATLR approach on temperature variations was considered a reasonable compromise at this investigation level. Also, few attempts to translate freeze-thaw cycles in quantitative terms and thresholds are present in the literature (D'Amato et al. 2016), and the results can be considered promising and with scope of improvement.

During spring, a high number of events were related to water inputs (both in the form of precipitation and WD episodes) plus FT cycles not ordinary conditions. Therefore, these occurrences could be explained through the processes described by Matsuoka (2008) and Draebing and Krautblatter (2019). According to these authors, rockfall can occur when water is available in cracks and joints (guaranteed by rainfall not ordinary conditions), and temperature conditions allow for frost wedging or ice segregation (guaranteed by FT cycles not ordinary conditions). Also, FT cycles alone are recognized as a highly frequent preparatory-triggering factor. Although the amplitude of thermal fluctuations of each cycle was not investigated in this work, in terms of processes, these occurrences could be related to repeated rock thermal stresses as described by Matsuoka (2019).

Only six rockfalls could not be associated to not ordinary conditions for the investigated climate indices. However, a preliminary exploratory analysis of these rockfalls suggested that they could be potentially referred to the occurrence of high temperatures and wide daily temperature gradients. Based on the elevations at which they took place, only a single rockfall could be referred to permafrost degradation (Matterhorn, 3735 m a.s.l., on August 04, 2003) as described by several authors working on high elevation rockfalls (Allen and Huggel 2013; Bodin et al. 2015; Paranunzio et al. 2016; Nigrelli et al. 2018). The event occurred at a medium-high elevation (1850 m a.s.l.) on June 05, 2009, could be possibly related to local episodes of late spring snow melting, as suggested by Paranunzio et al. (2016). The event recorded on July 09, 2017, at an elevation of 1175 m a.s.l., showed strong anomalies both in terms of high temperatures and temperature gradients; due to its elevation and date of occurrence, it fits well with the mechanism of thermal weathering described by Collins and Stock (2016) and Collins et al. (2018) and the thermal-related subcritical cracking described by Ishikawa et al. (2004). The same could be assumed for other three events, even if they had a weaker signal in terms of the effect of high temperatures and gradients. These few events are evidence of the growing effect of thermal fluctuations and extremely high temperatures on rock slope instabilities in the Alpine context. Having in mind the projected global warming, these preliminary results are therefore an indication that specific studies to enhance the knowledge related to these processes are necessary not only in arid and semiarid environments but over Alpine regions, too.

Conclusions

This work exploited the historical rockfall inventory and the meteorological stations database of Mont Cervin and Mont Emilius Mountain Communities (Aosta Valley, northern Italy) to decipher the interactions between climate and rock wall failures. The period from 1990 to 2018 was selected as reference to perform the analysis. Climate processes were translated into four climate indices, namely short-term rainfall (STR), effective water inputs (EWI, including both rainfall and snow melting), wet and dry episodes (WD) and freeze-thaw cycles (FT). Climate indices values, calculated for several pre-selected durations, were linked to rockfall occurrences and compared to the statistical distribution of each index. Critical percentiles (at least 75th) of the distributions were selected for each index to discern between ordinary and not ordinary climatic conditions. To validate the cause-effect relationship between the climatic conditions and rockfall occurrences, at least 50% of the rockfalls had to take place under not ordinary conditions. These not ordinary conditions were then used to derive empirical thresholds for the different indices. For threshold construction, if the critical percentile is exceeded for more than one duration, the lowest value was associated to the failure event to maintain a precautionary approach.
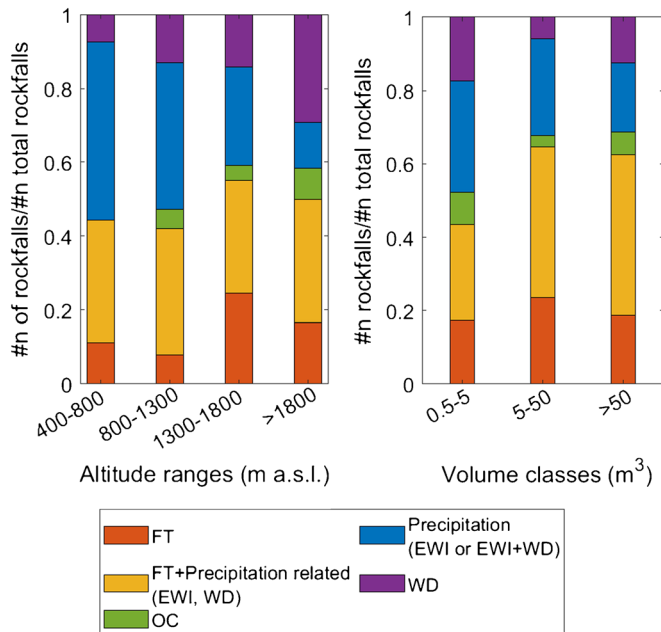
Fig. 13 Bar charts representing triggering and preparatory indices and their relationship with **a** altitude and **b** volume classes. Data are normalized to the total number of rockfalls belonging to each class to make classes comparable
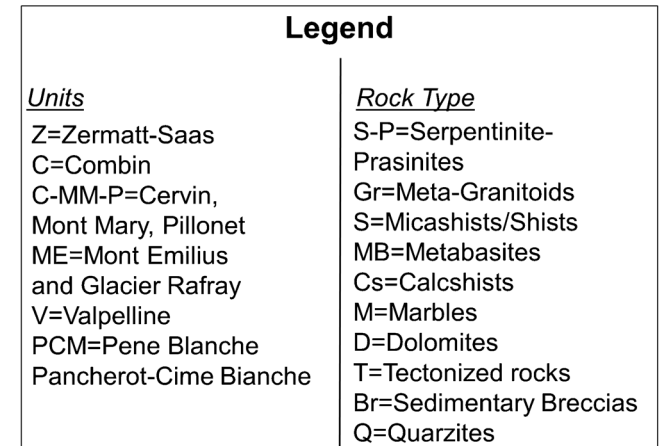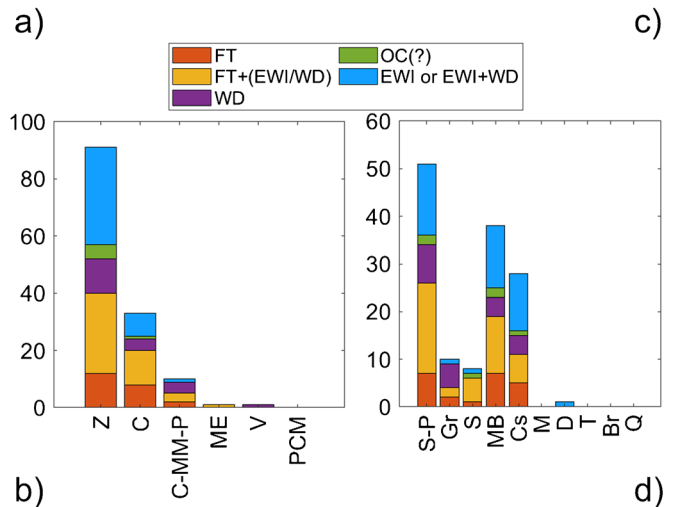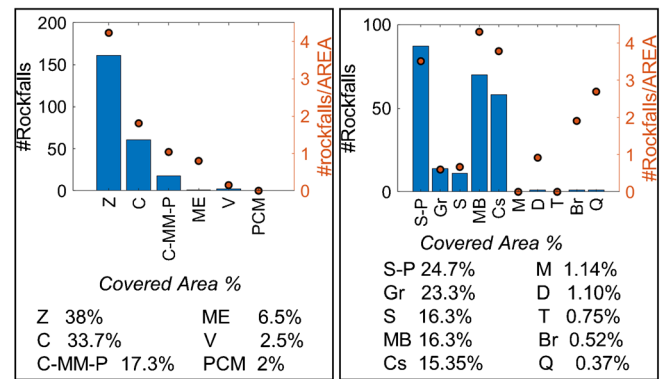

Fig. 14 Frequency of rockfalls (both precisely and not precisely dated) in relationship with **a** geological-structural underlying unit and **c** lithology. Dots represent the frequency of rockfalls divided by the percentage of the area covered by the unit (lithology). Bar charts representing triggering and preparatory indices and their relationship with **b** geological unit and **d** lithology/rock type

The most relevant findings of the study are:

(i) Out of the 168 rockfalls with available date of occurrence, 136 resulted to be comparable with meteorological data. Among these latter, more than 95% resulted to be associated to the occurrence of not ordinary climatic conditions for at least a climate index.

(ii) Among the four indices, only the STR resulted not significant, not meeting the procedure requirements (more than 50% of rockfalls occurred under not ordinary conditions). Nevertheless, the EWI index includes 1- to 7-day cumulated rainfall, thus considering the effect of short-term precipitation, too.

(iii) Not ordinary conditions for the EWI, WD and FT indices were recognized in correspondence of the 90th, 75th and 75th percentile value, respectively.

(iv) The combination of not ordinary conditions related to a precipitation index (either EWI, WD or both) and FT resulted as the most frequent climate situation leading to rockfalls in the study area. The second most frequent reason was related to not ordinary conditions in EWI, followed by not ordinary conditions in FT.

(v) Frequency of not ordinary conditions and indices association leading to rockfalls resulted to be reasonable with seasonality. FT cycles are particularly relevant in spring, while EWI is by far the most common influencing factor in autumn. As EWI contains snow deriving inputs, it is reasonable it resulted as the second most common influencing factor in spring.

(vi) For the EWI index, MAP- and RDN-normalized thresholds discriminate ordinary and not ordinary climate conditions better than the original data (i.e. not normalized ID threshold), having the advantage of reducing data dispersion and allowing to compare different precipitation regimes in the study area.

(vii) The normalization approach adopted for the freeze-thaw cycles threshold by introducing the FTN parameter did not improve the results as for EWI. A definition of temperature altitudinal lapse rate at more detailed temporal scales, or another normalization method, could lead to a more reliable threshold. Moreover, quantifying the intensity of

freeze (as in D'Amato et al. 2016, who used the freezing potential) may improve the analysis of freeze-thaw cycles.

(viii)   For the WD index, the threshold was designed through a global approach and no normalizations were further considered.

(ix)   A preliminary exploratory investigation of the role of high temperatures and temperature gradients showed that these factors can influence summertime rockfalls; these factors and the related processes should be further studied in light of the projected climate changes, particularly intense over the Alpine region.>

The procedure set up in this work could be applied in neighbouring regions. However, rock mass response to fatigue induced by climate processes also depends on local geomechanical conditions; thus, it is recommended to validate the presented thresholds or to develop local ones for different study areas. Dated rockfall events, which are rarely available, and a good spatial-temporal resolution of meteorological data are necessary to carry out a comparative analysis. For this reason, the efforts that some administrations (e.g. Aosta Valley region) are putting in developing not only spatial- but also temporal-detailed inventories are extremely important. The temporal information is the one that allows to analyse the influence on landslide occurrence of changing boundary conditions, such as climatic processes, land use and vegetation. This is fundamental to implement dynamic susceptibility, hazard and risk analyses, which are necessary in light of the climate changes affecting mountain environments. As for the outcomes of this study, it is expected that they will be used to set up a rockfall susceptibility analysis that will include, as spatially distributed predictors, summary variables derived from the relevant climate indices.

Data availability Meteorological and landslide data used in this work are freely accessible at https://cf.regione.vda.it/portale_dati.php and http://catastodissesti.partout.it/.

Declarations

Conflict of interest   The authors declare no competing interests.

References

Allen S, Huggel C (2013) Extremely warm temperatures as a potential cause of recent high mountain rockfall. Glob Planet Chang 107:59–69. https://doi.org/10.1016/j.gloplacha.2013.04.007

Amitrano D, Arattano M, Chiarle M, Mortara G, Occhiena C, Pirulli M, Scavia C (2010) Microseismic activity analysis for the study of the rupture mechanisms in unstable rock masses. Nat Hazards Earth Syst Sci 10:831–841. https://doi.org/10.5194/nhess-10-831-2010

Amitrano D, Gruber S, Girard L (2012) Evidence of frost-cracking inferred from acoustic emissions in a high-alpine rock-wall. Earth Planet Sci Lett 341–344:86–93. https://doi.org/10.1016/j.epsl.2012.06.014

Argand E (1911) Les nappes des recouvrement des Alpes Pennines et leur prolongements structuraux. Mat Carte Géol Suisse 31:1–26

Bakun-Mazor D, Hatzor YH, Glaser SD, Santamarina JC (2013) Thermally vs. seismically induced block displacements in Masada rock slopes. Int J Rock Mech Min Sci 61:196–211. https://doi.org/10.1016/j.ijrmms.2013.03.005

Bigi G, Castellarin A, Coli M, Dal Piaz GV, Sartori R, Scandone P & Vai GB, 1990. Structural Model of Italy scale 1:500.000, sheet 1. C.N.R., Progetto Finalizzato Geodinamica, SELCA Firenze

Bodin X, Schoeneich P, Deline P, Ravanel L, Magnin F, Krysiecki JM, Echelard T (2015) Mountain permafrost and associated geomorphological processes: recent changes in the French Alps. Revue De Geographie Alpine-journal of Alpine Research. https://doi.org/10.4000/rga.2885

Camera C, Bruggeman A, Hadjinicolaou P, Michaelides S, Lange MA (2017) Evaluation of a spatial rainfall generator for generating high resolution precipitation projections over orographically complex terrain. Stoch Env Res Risk A 31:757–773. https://doi.org/10.1007/s00477-016-1239-1

Collins BD, Stock GM (2016) Rockfall triggering by cyclic thermal stressing of exfoliation fractures. Nat Geosci 9:395–400. https://doi.org/10.1038/ngeo2686

Collins BD, Stock GM, Eppes M-C, Lewis SW, Corbett SC, Smith JB (2018) Thermal influences on spontaneous rock dome exfoliation. Nat Commun 9:762. https://doi.org/10.1038/s41467-017-02728-1

Crosta GB, di Prisco C, Frattini P, Frigerio G, Castellanza R, Agliardi F (2014) Chasing a complete understanding of the triggering mechanisms of a large rapidly evolving rockslide. Landslides 11:747–764. https://doi.org/10.1007/s10346-013-0433-1

Crozier MJ (2010) Deciphering the effect of climate change on landslide activity: a review. Geomorphology 124:260–267. https://doi.org/10.1016/j.geomorph.2010.04.009

D'Amato J, Hantz D, Guerin A, Jaboyedoff M, Baillet L, Mariscal A (2016) Influence of meteorological factors on rockfall occurrence in a middle mountain limestone cliff. Nat Hazards Earth Syst Sci 16:719–735. https://doi.org/10.5194/nhess-16-719-2016

Dal Piaz G, Cortiana G, Del Moro A, Martin S, Pennacchioni G, Tartarotti P (2001) Tertiary age and paleostructural inferences of the eclogitic imprint in the Austroalpine outliers and Zermatt–Saas ophiolite, western Alps. Int J Earth Sci 90:668–684. https://doi.org/10.1007/s005310000177

Delonca A, Gunzburger Y, Verdel T (2014) Statistical correlation between meteorological and rockfall databases. Nat Hazards Earth Syst Sci 14:1953–1964. https://doi.org/10.5194/nhess-14-1953-2014

DeWalle DR, Rango A (2008) Principles of snow hydrology. Cambridge University Press, New York, 410pp. https://doi.org/10.1657/1938-4246-41.4.523, David R.

Draebing D, Krautblatter M (2019) The efficacy of frost weathering processes in Alpine rockwalls. Geophys Res Lett 46:6516–6524. https://doi.org/10.1029/2019GL081981

Draebing D, Haberkorn A, Krautblatter M, Kenner R, Phillips M (2017a) Thermal and mechanical responses resulting from spatial and temporal snow cover variability in permafrost rock slopes, Steintaelli, Swiss Alps. Permafr Periglac Process 28:140–157. https://doi.org/10.1002/ppp.1921

Draebing D, Krautblatter M, Hoffmann T (2017b) Thermo-cryogenic controls of fracture kinematics in permafrost rockwalls. Geophys Res Lett 44:3535–3544. https://doi.org/10.1002/2016GL072050

Duvillard PA, Ravanel L, Deline P (2015) Risk assessment of infrastructure destabilisation due to global warming in the high French Alps. Journal of Alpine Research| Revue de géographie alpine 103:2. https://doi.org/10.4000/rga.2896

Ellero A, Loprieno A (2017) Nappe stack of Piemonte–Ligurian units south of Aosta Valley: new evidence from Urtier Valley (Western Alps). Geol J 53:1665–1684. https://doi.org/10.1002/gj.2984

Frayssines M, Hantz D (2006) Failure mechanisms and triggering factors in calcareous cliffs of the Subalpine Ranges (French Alps). Eng Geol 86:256–270. https://doi.org/10.1016/j.enggeo.2006.05.009

Gariano SL, Guzzetti F (2016) Landslides in a changing climate. Earth Sci Rev 162:227–252. https://doi.org/10.1016/j.earscirev.2016.08.011

Giordan D, Cignetti M, Wrzesniak A, Allasia P, Bertolo D (2018) Operative monographies: development of a new tool for the effective management of landslide risks. Geosciences 8. https://doi.org/10.3390/geosciences8120485

Gunzburger Y, Merrien-Soukatchoff V, Guglielmi Y (2005) Influence of daily surface temperature fluctuations on rock slope stability: case study of the Rochers de Valabres slope (France). Int J Rock Mech Min Sci 42(3):331–349. https://doi.org/10.1016/j.ijrmms.2004.11.003

Guyennon N, Valt M, Salerno F, Petrangeli AB, Romano E (2019) Estimating the snow water equivalent from snow depth measurements in the Italian Alps. Cold Reg Sci Technol 167:102859. https://doi.org/10.1016/j.coldregions.2019.102859

Guzzetti F (2000) Landslide fatalities and the evaluation of landslide risk in Italy. Eng Geol 58:89–107. https://doi.org/10.1016/S0013-7952(00)00047-8

Guzzetti F, Peruccacci S, Rossi M, Stark CP (2007) Rainfall thresholds for the initiation of landslides in central and southern Europe. Meteorog Atmos Phys 98:239–267. https://doi.org/10.1007/s00703-007-0262-7

Guzzetti F, Peruccacci S, Rossi M, Stark CP (2008) The rainfall intensity–duration control of shallow landslides and debris flows: an update. Landslides 5:3–17. https://doi.org/10.1007/s10346-007-0112-1

Guzzetti F, Mondini AC, Cardinali M, Fiorucci F, Santangelo M, Chang K-T (2012) Landslide inventory maps: new tools for an old problem. Earth Sci Rev 112:42–66. https://doi.org/10.1016/j.earscirev.2012.02.001

Hales TC, Roering JJ (2007) Climatic controls on frost cracking and implications for the evolution of bedrock landscapes. J Geophys Res Earth Surf 112. https://doi.org/10.1029/2006JF000616

Hartmeyer I, Delleske R, Keuschnig M, Krautblatter M, Lang A, Schrott L, Otto J-C (2020) Current glacier recession causes significant rockfall increase: the immediate paraglacial response of deglaciating cirque walls. Earth Surf Dyn Discuss 2020:1–25. https://doi.org/10.5194/esurf-2020-8

Hasler A, Gruber S, Beutel J (2012) Kinematics of steep bedrock permafrost. J Geophys Res Earth Surf 117. https://doi.org/10.1029/2011JF001981

He ZH, Parajka J, Tian FQ, Blöschl G (2014) Estimating degree-day factors from MODIS for snowmelt runoff modeling. Hydrol Earth Syst Sci 18:4773–4789. https://doi.org/10.5194/hess-18-4773-2014

Hungr O, Leroueil S, Picarelli L (2014) The Varnes classification of landslide types, an update. Landslides 11:167–194. https://doi.org/10.1007/s10346-013-0436-y

Ishikawa M, Kurashige Y, Hirakawa K (2004) Analysis of crack movements observed in an alpine bedrock cliff. Earth Surf Process Landf 29:883–891. https://doi.org/10.1002/esp.1076

Kegang L, Lin M, Xiangxing L, Shoujian P (2016) Effect of drying-wetting cycles on triaxial compression mechanical properties of sandstone. J Eng Sci Technol Rev 9(3):66–73. https://doi.org/10.25103/jestr.093.10

Kirchner M, Faus-Kessler T, Jakobi G, Leuchner M, Ries L, Scheel H-E, Suppan P (2013) Altitudinal temperature lapse rates in an Alpine valley: trends and the influence of season and weather patterns. Int J Climatol 33:539–555. https://doi.org/10.1002/joc.3444

Krautblatter M, Draebing D (2014) Pseudo 3-D P wave refraction seismic monitoring of permafrost in steep unstable bedrock. J Geophys Res Earth Surf 119:287–299. https://doi.org/10.1002/2012JF002638

Krautblatter M, Moser M (2009) A nonlinear model coupling rockfall and rainfall intensity based \newline on a four year measurement in a high Alpine rock wall (Reintal, German Alps). Nat Hazards Earth Syst Sci 9:1425–1432. https://doi.org/10.5194/nhess-9-1425-2009

Leonarduzzi E, Molnar P (2020) Data limitations and potential of hourly and daily rainfall thresholds for shallow landslides. Nat Hazards Earth Syst Sci Discuss 2020:1–25. https://doi.org/10.5194/nhess-2020-125

Macciotta R, Martin CD, Edwards T, Cruden DM, Keegan T (2015) Quantifying weather conditions for rock fall hazard management. Null 9:171–186. https://doi.org/10.1080/17499518.2015.1061673

Macciotta R, Hendry M, Cruden DM, Blais-Stevens A, Edwards T (2017) Quantifying rock fall probabilities and their temporal distribution associated with weather seasonality. Landslides 14:2025–2039. https://doi.org/10.1007/s10346-017-0834-7

Matsuoka N (2001) Direct observation of frost wedging in alpine bedrock. Earth Surf Process Landf 26:601–614. https://doi.org/10.1002/esp.208

Matsuoka N (2008) Frost weathering and rockwall erosion in the southeastern Swiss Alps: long-term (1994–2006) observations. Geomorphology 99:353–368. https://doi.org/10.1016/j.geomorph.2007.11.013

Matsuoka N (2013) Time-lapse photography applied to monitoring of alpine slope processes. Tsukuba Geoenviron Sci 9:13–19

Matsuoka N (2019) A multi-method monitoring of timing, magnitude and origin of rockfall activity in the Japanese Alps. Geomorphology 336:65–76. https://doi.org/10.1016/j.geomorph.2019.03.023

Nigrelli G, Fratianni S, Zampollo A, Turconi L, Chiarle M (2018) The altitudinal temperature lapse rates applied to high elevation rockfalls studies in the Western European Alps. Theor Appl Climatol 131:1479–1491. https://doi.org/10.1007/s00704-017-2066-0

Nishii R, Matsuoka N, Daimaru H, Yasuda M (2013) Precursors and triggers of an alpine rockslide in Japan: the 2004 partial collapse during a snow-melting period. Landslides 10:75–82. https://doi.org/10.1007/s10346-012-0353-5

Paranunzio R, Laio F, Nigrelli G, Chiarle M (2015) A method to reveal climatic variables triggering slope failures at high elevation. Nat Hazards 76:1039–1061. https://doi.org/10.1007/s11069-014-1532-6

Paranunzio R, Laio F, Chiarle M, Nigrelli G, Guzzetti F (2016) Climate anomalies associated with the occurrence of rockfalls at high-elevation in the Italian Alps. Nat Hazards Earth Syst Sci 16:2085–2106. https://doi.org/10.5194/nhess-16-2085-2016

Paranunzio R, Chiarle M, Laio F, Nigrelli G, Turconi L, Luino F (2019) New insights in the relation between climate and slope failures at high-elevation sites. Theor Appl Climatol 137:1765–1784. https://doi.org/10.1007/s00704-018-2673-4

Peruccacci S, Brunetti MT, Gariano SL, Melillo M, Rossi M, Guzzetti F (2017) Rainfall thresholds for possible landslide occurrence in Italy. Geomorphology 290:39–57. https://doi.org/10.1016/j.geomorph.2017.03.031

Petschko H, Brenning A, Bell R, Goetz J, Glade T (2014) Assessing the quality of landslide susceptibility maps – case study Lower Austria. Nat Hazards Earth Syst Sci 14:95–118. https://doi.org/10.5194/nhess-14-95-2014

Petschko H, Bell R, Glade T (2016) Effectiveness of visually analyzing LiDAR DTM derivatives for earth and debris slide inventory mapping for statistical susceptibility modeling. Landslides 13:857–872. https://doi.org/10.1007/s10346-015-0622-1

Pistocchi A (2016) Simple estimation of snow density in an Alpine region. J Hydrol Reg Stud 6:82–89. https://doi.org/10.1016/j.ejrh.2016.03.004

Ponziani M, Pogliotti P, Stevenin H, Ratto SM (2020) Debris-flow indicator for an early warning system in the Aosta valley region. Nat Hazards 104:1819–1839. https://doi.org/10.1007/s11069-020-04249-5

Ratto S, Bonetto F, Comoglio C (2003) The October 2000 flooding in Valle d'Aosta (Italy): event description and land planning measures for the risk mitigation. Int J River Basin Manag 1:105–116. https://doi.org/10.1080/15715124.2003.9635197

Ravanel L, Deline P (2010) Climate influence on rockfalls in high-Alpine steep rockwalls: the north side of the Aiguilles de Chamonix (Mont Blanc massif) since the end of the 'Little Ice Age. The Holocene 21:357–365. https://doi.org/10.1177/0959683610374887

Ravanel L, Deline P, Lambiel C, Vincent C (2013) Instability of a high alpine rock ridge: the Lower Arête Des Cosmiques, Mont Blanc Massif, France. Geogr Ann Ser A Phys Geogr 95:51–66

Reichenbach P, Rossi M, Malamud BD, Mihir M, Guzzetti F (2018) A review of statistically-based landslide susceptibility models. Earth Sci Rev 180:60–91. https://doi.org/10.1016/j.earscirev.2018.03.001

Rolland C (2003) Spatial and seasonal variations of air temperature lapse rates in Alpine regions. J Clim 16:1032–1046. https://doi.org/10.1175/1520-0442(2003)016<1032:SASVOA>2.0.CO;2

Rubel F, Brugger K, Haslinger K, Auer I (2017) The climate of the European Alps: Shift of very high resolution Köppen-Geiger climate zones 1800–2100. Meteorologische Zeitschrift 26(2):115–125

Scavia C, Barbero M, Castelli M, Marchelli M, Peila D, Torsello G, Vallero G (2020) Evaluating rockfall risk: some critical aspects. Geosciences 10. https://doi.org/10.3390/geosciences10030098

Seibert J, Jenicek M, Huss M, Ewen T (2015) Chapter 4 - Snow and ice in the hydrosphere. In: Shroder JF, Haeberli W, Whiteman C (eds) Snow and Ice-Related Hazards, Risks and Disasters. Academic Press, Boston, pp 99–137. https://doi.org/10.1016/B978-0-12-394849-6.00004-4

Steger S, Brenning A, Bell R, Glade T (2016) The propagation of inventory-based positional errors into statistical landslide susceptibility models. Nat Hazards Earth Syst Sci 16:2729–2745. https://doi.org/10.5194/nhess-16-2729-2016

Stoffel M, Tiranti D, Huggel C (2014) Climate change impacts on mass movements — case studies from the European Alps. Sci Total Environ 493:1255–1266. https://doi.org/10.1016/j.scitotenv.2014.02.102

Strunden J, Ehlers TA, Brehm D, Nettesheim M (2015) Spatial and temporal variations in rockfall determined from TLS measurements in a deglaciated valley, Switzerland. J Geophys Res Earth Surf 120:1251–1273. https://doi.org/10.1002/2014JF003274

Torres-Suarez MC, Alarcon-Guzman A, Moya R, Berdugo D (2014) Effects of loading–unloading and wetting–drying cycles on geomechanical behaviors of mudrocks in the Colombian Andes. J Rock Mech Geotech Eng 6:257–268. https://doi.org/10.1016/j.jrmge.2014.04.004

USDA-NEH, (2004)- National Engineering Handbook Chapter 11 Part 630 United States Department of Agriculture Natural Resources Conservation Service

Van der Hoven SJ, Solomon DK, Moline GR (2003) Modeling unsaturated flow and transport in the saprolite of fractured sedimentary rocks: effects of periodic wetting and drying. Water Resour Res 39:39. https://doi.org/10.1029/2002WR001926

Vargas EA, Velloso RQ, Chávez LE, Gusmão L, do Amaral CP (2013) On the effect of thermally induced stresses in failures of some rock slopes in Rio de Janeiro, Brazil. Rock Mech Rock Eng 46:123–134. https://doi.org/10.1007/s00603-012-0247-9

Weber S, Beutel J, Faillettaz J, Hasler A, Krautblatter M, Vieli A (2017) Quantifying irreversible movement in steep, fractured bedrock permafrost on Matterhorn (CH). Cryosphere 11:567–583. https://doi.org/10.5194/tc-11-567-2017

World Meteorological Organization, 1989: Calculation of monthly and annual 30-year standard normals. WCDP-No. 10, WMO-TD/No. 341, World Meteorological Organization.

World Meteorological Organization, 2007: The role of climatological normals in a changing climate. WCDMP-No. 61, WMO-TD/No. 1377, World Meteorological Organization.

Yang X, Wang J, Hou D, Zhu C, He M (2018) Effect of dry-wet cycling on the mechanical properties of rocks: a laboratory-scale experimental study. Processes 6. https://doi.org/10.3390/pr6100199

Yang X, Wang J, Zhu C, He M, Gao Y (2019) Effect of wetting and drying cycles on microstructure of rock based on SEM. Environ Earth Sci 78:183. https://doi.org/10.1007/s12665-019-8191-6

Zhou Z, Cai X, Chen L, Cao W, Zhao Y, Xiong C (2017) Influence of cyclic wetting and drying on physical and dynamic compressive properties of sandstone. Eng Geol 220:1–12. https://doi.org/10.1016/j.enggeo.2017.01.017

Zimmer VL, Sitar N (2015) Detection and location of rock falls using seismic and infrasound sensors. Eng Geol 193:49–60. https://doi.org/10.1016/j.enggeo.2015.04.007

G. Bajni (✉) · **C. A. S. Camera** · **T. Apuani**
Dipartimento di Scienze della Terra "A. Desio",
Università degli Studi di Milano,
Via Mangiagalli 34, 20133, Milan, Italy
Email: greta.bajni@unimi.it